T2R2 東京科学大学 リサーチリポジトリ
Science Tokyo Research Repository

論文 / 著書情報
Article / Book Information

題目(和文)	
Title(English)	Modification of ZSM-5 Zeolite and Its Catalytic Properties
著者(和文)	KARIMTahta Muslim
Author(English)	Tahta Muslim Karim
出典(和文)	学位:博士(工学), 学位授与機関:東京工業大学, 報告番号:甲第12873号, 授与年月日:2024年9月20日, 学位の種別:課程博士, 審査員:横井 俊之,多湖 輝興,山口 猛央,松本 秀行,原田 琢也
Citation(English)	Degree:Doctor (Engineering), Conferring organization: Tokyo Institute of Technology, Report number:甲第12873号, Conferred date:2024/9/20, Degree Type:Course doctor, Examiner:,,,,
学位種別(和文)	博士論文
Category(English)	Doctoral Thesis
種別(和文)	要約
Type(English)	Outline

Powered by T2R2 (Science Tokyo Research Repository)

Thesis outline

Modification of ZSM-5 Zeolite and Its Catalytic Properties

Department of Chemical Science and Engineering

School of Material and Chemical Technology

Tokyo Institute of Technology

Tahta Muslim Karim

Chapter 1:

General Introduction

1.1. Zeolite

1.1.1. Introduction of zeolite

Zeolite is the microporous crystalline aluminosilicates that is composed of TO_4 tetrahedra (T = Si, Al) with O as a bridge connecting neighboring tetrahedra. For a completely siliceous structure, the combination of TO_4 tetrahedra (T = Si) units results in the silica framework which is an uncharged solid. When incorporation of Al (Al charge of +3) into the silica framework, it gives rise to the framework becoming the negative charge so that requiring the presence of extra-framework cations to balance this charge to keep the overall framework neutral. Therefore, the zeolite composition can be described as follows [1],[2]:

$$M_x \cdot [Si_{(t-x)}Al_xO_{2t}] \cdot yH_2O$$

extra-framework cations framework adsorbed phase

where M represents a univalent charge-balancing cation, *x* is the number of framework Al atoms in the unit cell, *y* is the number of adsorbed water molecules, *t* is the total number of framework tetrahedral atoms in the unit cell (Al + Si).

The extra-framework cations are ion exchangeable so that it leads the zeolite can be used as an ion-exchange material. Meanwhile, the amount of Al in the zeolite framework can vary in a wide range, from Si/Al = 1 to infinity which is the completely siliceous form. Since increasing the Si/Al ratio of the framework, then the hydrothermal stability and hydrophobicity of zeolite increase as well. On the other hand, in as-synthesized zeolite, typically water involved during the synthesis occupies the internal void of the zeolite [2]. Its adsorbed phase is able to be removed by the thermal treatment which makes the intracrystalline space available. Since the crystalline nature of the framework makes sure the pore openings are uniform throughout the crystal, the zeolite can discriminate the molecules with the dimensional difference causing it also be named by molecular sieves.

In the zeolite structure, the basic structural units (AlO_4 or SiO_4) are assembled becoming the secondary building units that may be simple polyhedral, such as cubes and hexagonal prisms. Then, those secondary building units are assembled to form the final framework. Therefore, the framework structure contains channels exhibiting pore size from 0.3 to 1.0 nm and pore volume from about 0.10 to 0.35 cm^3/g [1]. So that, the zeolite pore sizes are classified to be typical four classes: (1) small pores with eight-ring pores; (2) medium pores with 10-ring pores; (3) large pores with 12-ring pores; (4) extra-large pores with 14-ring pores [1].

1.1.2. Zeolite porosity

The process to reach the intracrystalline void of zeolites occurred via rings which composed of T (Si, Al) and O atoms. For six-membered rings (6-MR) or less, the window is ~ 2 Å [2], so that the movement of species through these rings is limited. Ions or molecules are able to be trapped in this size or smaller. While, for zeolites containing larger rings (8-MR, 10-MR, etc), those species can enter the intracrystalline space easily. Figure 1.1 shows the range of porosity typically found in zeolites, in which diffusivities can change up to 12x magnitude depending on the pore size and the size and shape of the diffused molecules into zeolite [3].

The internal structure of zeolite comprising of interconnected cages or channels that can have dimensionalities of one to three [2]. The framework is able to perform somewhat flexible with changes in temperature and through guest molecule-host interaction, as shown for the orthorhombic-monoclinic transformation [4].

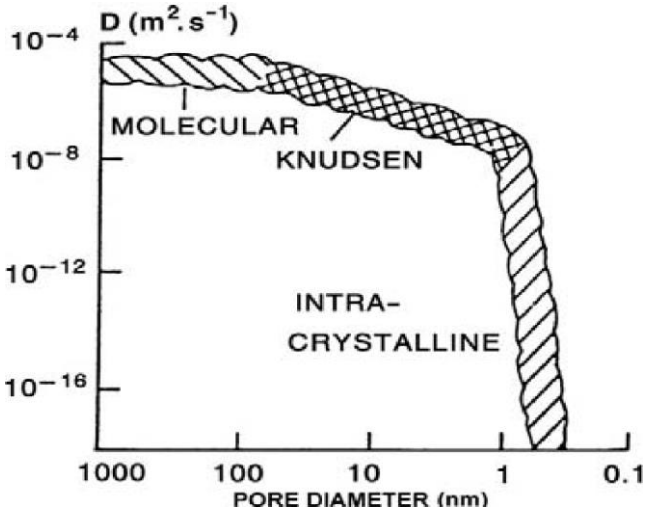

Figure 1.1. Effect of pore diameter on molecular diffusivity [3].

The rigid pore structure gives rise to steric constraints on the molecules in the zeolite causing new reaction pathways when compared to unconstrained media [2]. As shown in Figure 1.2, it is the examples of reactant, product, and transition state selectivities [5], that the increase of size upon methyl substitution results in prevention the alkane to enter the zeolite. Furthermore, the diffusivity of p-xylene is higher a few magnitude in the channel system of zeolite compared to the ortho and meta isomers facilitating selectivity on the product.

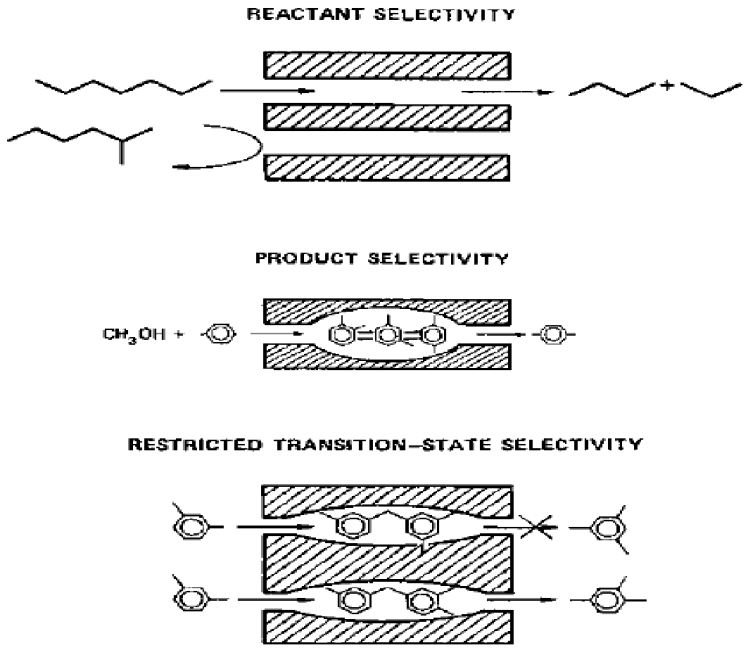

Figure 1.2. Different types of reaction selectivity caused by the rigid pore structure of zeolite [5].

1.1.3. Zeolite framework structure

1.1.3.1. Basic building unit

The zeolite frameworks are constructed by linking in a periodic pattern a basic building unit (BBU), the tetrahedron. In the core of the tetrahedra are atoms having the relatively low electronegativities and in the corners are oxygen anion [2]. These combinations result in species like [SiO_4] and [AlO_4] which is usually written as TO_4 to describe tetrahedra in general, in which T stands for any tetrahedral species. Sometimes, it is written in the notation [$TO_{4/2}$] for emphasizing that each oxygen atom coordinated to two T atoms. Figure 1.3 represents several representations of the tetrahedron.

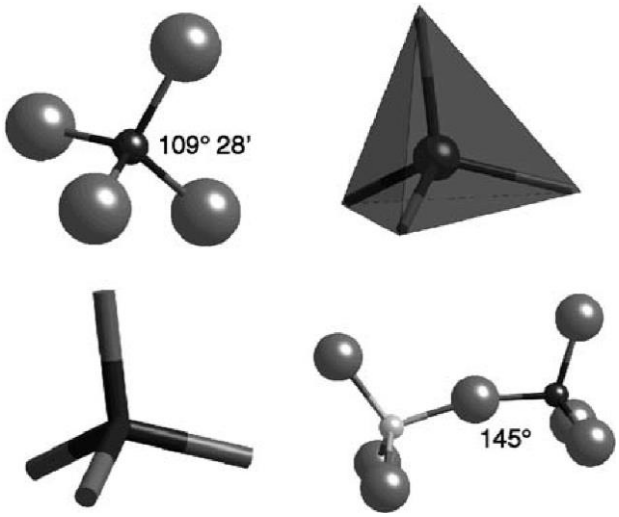

Figure 1.3. Several representations of the basic building unit of zeolites, the tetrahedron [2].

The tetrahedra are linked through the apical oxygen (T-O-T) to build zeolite framework [2]. The T-O-T bond angle is quite flexible [6],[7],[8], in dramatic contrast to the rigid O-T-O angle. For the case of silica tetrahedra, the T-O-T angle is usually in the range of 140 – 165^0, but values have been reported of 130 – 180^0 [6]. The flexibility of the T-O-T angle is very important since the degree of flexibility resulting in the formation of many variants of zeolite

frameworks without huge thermodynamic penalty [9],[10]. Furthermore, the flexibility of the T-O-T angle permits the ring formations and other more complex building units [2].

1.1.3.2. Composite building units

Composite building units (CBUs) are built by linking together groups of BBUs. The simples examples of CBUs are rings, and all zeolite structures are formed from the rings of tetrahedra of different sizes [2]. Generally, a ring containing *x* tetrahedra called an *x* ring. While, when a ring defines the face of a polyhedral unit, it is also called a window [2]. Figure 1.4 demonstrates several examples of the relative sizes of some *x* rings.

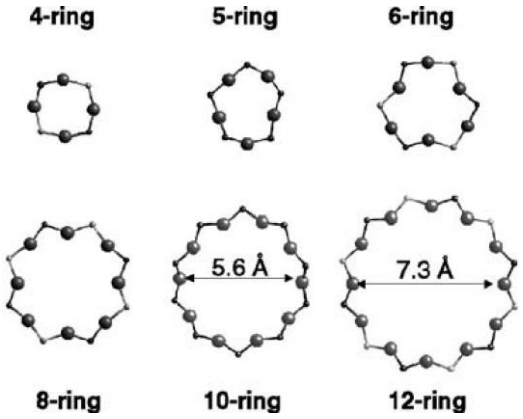

Figure 1.4. Relative sizes of *x*-rings frequently found in zeolites [2].

More complex CBUs are achieved by assembling several CBUs to build larger CBUs giving rise to formation a certain structure, like cage or chain. Cages are polyhedral whose largest rings are too narrow to permit the causeway of molecules larger than water, and it is usually considered that 6-rings are the limitation of the ring size for forming a cage [2]. Figure 1.5 shows the example of cage varieties. Meanwhile, chains are one-dimensional polyhedral CBUs which are often found among structures of zeolite [2]. Figure 1.6 depicts two examples of chains from ZSM-5 (MFI) and L (LTL) zeolites, respectively. They can be seen that ZSM-5 zeolite (MFI) is constructed by connecting 5-rings while L zeolite (LTL) is formed from 4-rings, 6-rings, and 8 rings.

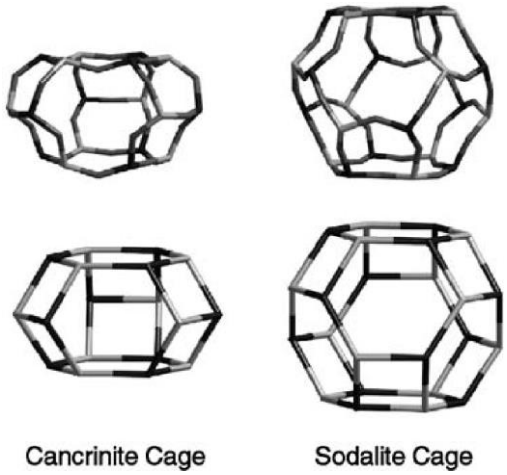

Figure 1.5. Two cages found in zeolites frequently. Oxygen and T atoms are demonstrated in the above drawings, and in the under one, only the connections between T-atoms are indicated [2].

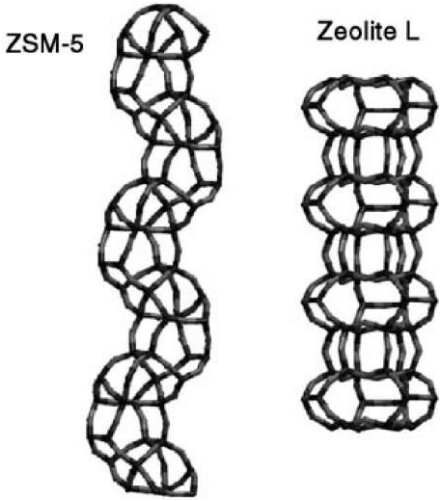

Figure 1.6. illustrates the chains are frequently found in zeolite structures [2].

1.1.4. Property

Many industrial conversion processes carry out in the presence of catalysts which is able to accelerate the speed of conversion and address the selectivity towards the most wanted products. Zeolite as a solid acid catalyst emerges to answer the industry's desire because it has strong acid sites and shape selectivity. Therefore, now, zeolite is widely used in many

industries, such as petrochemical industry. Because these properties are very important, then they will be further explained here.

1.1.4.1. Shape selectivity

The concept of shape selectivity was proposed for the first time by Weiz and Frilette [11],[12] at around 1960s for explaining the unexpected results that gained with calcium-ion-exchange zeolite. Since then, a lot of studies undertaken, and it had led to the discovery of new forms of shape selectivity and allowing to obtain a deeper understanding of the complex interactions carrying out between the porous structure of zeolites and the reacting system [13]. Now, many theories proposed to explain the different finding, but the most widely accepted theories to explain the shape selectivity are reported as follows:

1. Reactant Shape Selectivity (RSS)

This type of selectivity happens while the presence of difference in reactivity between two competing molecules which caused by their different accessibility to go into the internal active sites of the zeolite [13]. While the pore opening of the zeolite is similar to the size of the reactant molecule, a small difference in the diameter of the reactant molecule will cause a change of its diffusion by order of magnitude and in the extreme case, it will be hindered to go to the internal surface [14]. This case is shown in Figure 1.7, in which only molecule having a small enough diameter that can enter the porous structure and then it will react, while the bulkier molecules will be rejected and leaving the system unchanged.

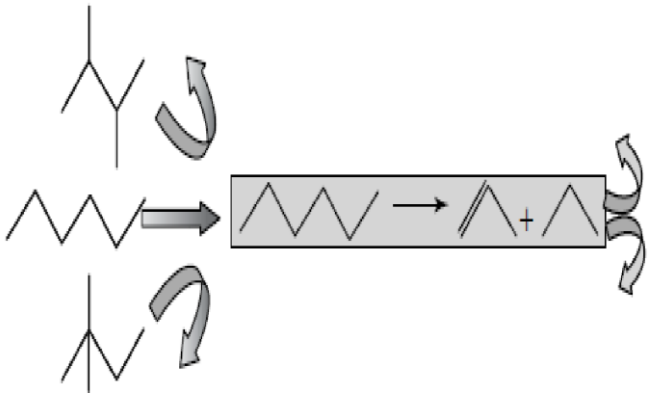

Figure 1.7. Example of reactant shape selectivity: the selective cracking of *n*-hexane in the presence of *i*-hexanes [13].

2. Product Shape Selectivity (PSS)

For this type of selectivity, the reactants are small enough to diffuse easily via the channels of the zeolite, but among all the possible products that can be formed, only the products with a small enough size (in relation to the pore size) are able to diffuse more or less rapidly and leaving the zeolite structure [13]. Figure 1.8 demonstrates the example of product shape selectivity.

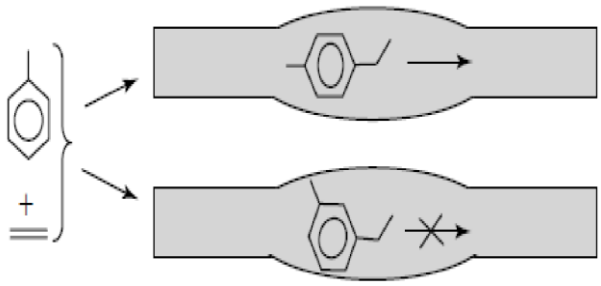

Figure 1.8. Example of product shape selectivity: suppression of trimethylbenzene during *meta*-xylene isomerization [15].

3. Transition State Shape Selectivity (TSS)

This type refers to the condition where the lack of space around the active sites hinders the formation of transition states which is spatially constrained either by their size or their orientation [13]. Figure 1.9 illustrates the example of the transition state shape selectivity.

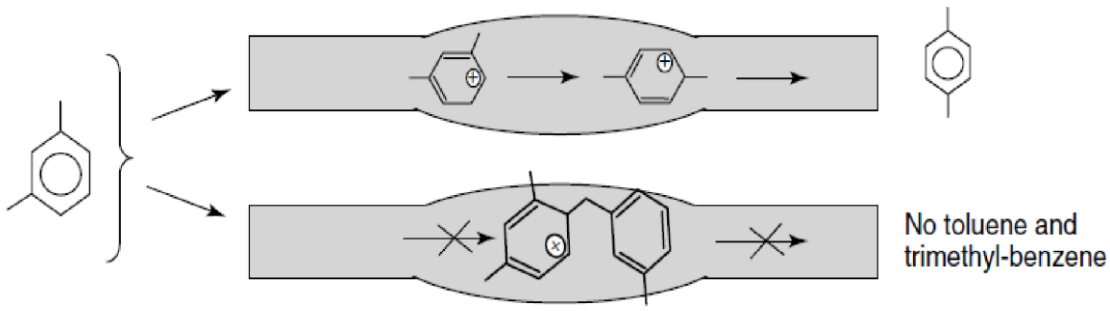

Figure 1.9. Example of transition state shape selectivity: formation of *para*-ethyl toluene with ethylene [13].

Another example for the transition state shape selectivity is 3-methylpentane cracking on ZSM-5 zeolite as reported by Haag, et.al. [16]. They evaluated diffusion inhibition of the reaction rate based on the effect of mass transport-induced selectivity which created by steric hindrance by the size of a reaction complex, in which they did the tests by catalytic cracking of C_6 to C_9 hydrocarbons. They reported the selective cracking of *n*-paraffins compared to monomethyl paraffins was because of a higher intrinsic rate constant of the *n*-paraffins, in which diffusional mass transport did not give a huge effect. On the contrary, dimethyl paraffin cracking was strongly diffusion-hindered. Furthermore, it was found that the methyl paraffin/*n*-paraffin discrimination was a result of the steric constraint on the sizeable methyl paraffin/carbonium ion reaction complex (transition state) (Figure 1.10). Based on these findings, constraint index (CI) emerges as a test reaction to investigate the relative pore sizes and shape selective properties of acidic zeolites [17].

The constraint index (CI) is ratio of the reaction rates of *n*-hexane cracking and 3-metylpentane cracking. A higher CI value appears from the preferable cracking of *n*-hexane compared to the its branched isomer because 3-methylpentane would be easier cracked in the absence of the steric constraints [17]. The pore classification involving CI are categorized as: CI value < 1 is for large pores; if the CI value 1 < CI < 12, then it is for intermediate pores; while CI > 12 is for small pores [2].

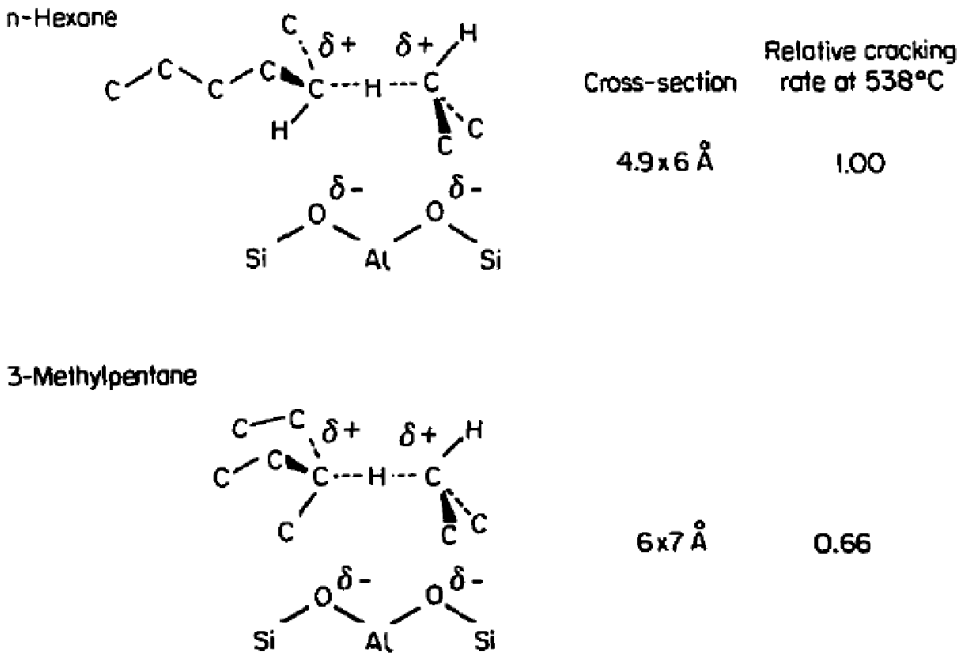

Figure 1.10. Dimensions of transition states of C_6 paraffins [5].

Beside the concepts has been mentioned above (they are called the classical concepts), the new concepts of the shape selectivity have been emerged to explain the different experimental results. Those concepts are molecular traffic control, pore-mouth and key-lock selectivity, window effect, and nest effect [18].

1.1.4.2. Acid sites

In aluminosilicate-type zeolites, the +4 charges on framework silicon atoms at T position and the -2 charges on the connecting oxygen atoms lead to neutral $SiO_{4/2}$ tetrahedra. When substitution of silicon atoms in the framework replaced by the metal atoms with a +3 charge, typically by aluminum atoms, the formal charge of the corresponding tetrahedra changes to be -1 ($AlO_{4/2}^-$). The charge of these negative frameworks are balanced by extra-framework metal cations or hydroxyl protons that form the weak Lewis acid sites or strong Brønsted acid sites, respectively, which is responsible for the catalytic activity of the zeolites [19]. The hydroxyl protons are located on the oxygen bridges that connect the tetrahedrally coordinated framework silicon and aluminum atoms as shown in Figure 1.11 (a). These hydroxyl groups are frequently expressed as the structural or bridging OH groups (SiOHAl).

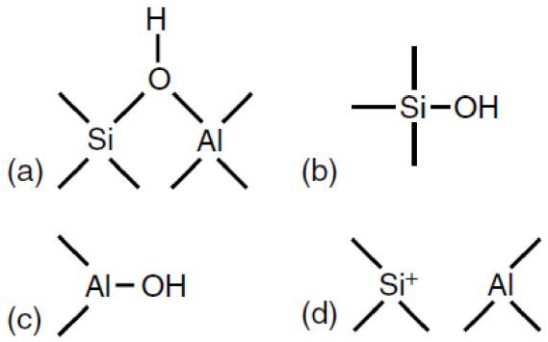

Figure 1.11. Schematic representation of the different types of hydroxyl groups and acid sites in zeolites [13].

In the mesoporous material with amorphous walls, like MCM-41, MCM-48, SBA-15, dan FSM-16, the brønsted acid sites are most likely emerges from sites with local structures similar to bridging OH groups in zeolites [20],[21],[22]. The best illustration of these sites are weakly bound protons of SiOH groups at tetrahedrally coordinated silicon atoms that interact with neighboring atoms which act as lewis acid sites, that means as electron pair acceptors, like aluminum atoms [13]. While in the case of zeolites, the Si – O – Al bridging bonds are closed, even in the activated state of material. Whereas, in the mesoporous materials with amorphous wall and the same arrangement as mentioned above, the O – Al distance is much larger than in crystalline zeolite that lead to characteristics of SiOH groups with neighboring lewis sites, especially in the activated state [23].

The second important type of hydroxyl groups are the silanol groups (SiOH) which is called terminal OH groups, that located on the external surface of crystal particles or at the defects of framework (Figure 1.11 (b)). Formation of framework defects and silanol groups can be occurred by many aspects, for instance dealumination of zeolite by calcination, hydrothermal treatment or treatment with strong acids [13]. Depending on the treatment conditions, healing of framework defects may be occurred, like by silicon migration, formation

of silanol groups, or formation of hydroxyl groups at extra-framework aluminum species (Figure 1.11 (c)) [19].

In dealumination of the zeolite framework, it is often accompanied by the formation of lewis acid sites at extra-framework species and framework defects (Figure 1.11 (d)). If those lewis acid sites located at around bridging OH groups, for example, in the framework of weakly steamed zeolite, the superacidic brønsted sites are going to be formed [24]. Furthermore, Lago and co-workers reported the catalytic activity in the n-hexane cracking on H-ZSM-5 zeolite was strongly increased, which was attributed to the superacidic brønsted sites that formed when mild steaming [25]. Those sites were explained by a partial hydrolyzation of framework aluminum atoms that act as lewis acid sites at around bridging OH groups (SiOHAl), in which those lewis acid sites act as the strong electron attracting centers for neighboring bridging OH groups and creating brønsted acid sites with very high strength. However, at the same time, the similar effects were occurred as well for bridging OH groups at around of extra-framework aluminum species acting as lewis acid sites [26].

1.2. The hierarchical zeolite

A variety of methods for creating the hierarchical zeolites has been developed the last decades. In general, the methods can be divided into two main groups, i.e., 1) the top-down and 2) the bottom-up methods. Nowadays, the third class of hierarchical system has appeared, i.e., nanozeolites and their assemblies. This approach can be produced using both top-down and bottom-up methods so that, sometimes, it called the mixed method.

1.2.1. Top-down methods

In principle, top-down methods begin with existing microporous zeolites, synthesized in advance or commercially available, that are then post synthetically modified for creating the hierarchical zeolite structures [27]. There are several techniques that commonly used to create

the hierarchical structure via this method, such as dealumination, desilication, and dissolution-recrystallization [28].

1. Dealumination

Dealumination is the first technique used (1960s) for introducing mesopores in a zeolite by removing Al from the zeolite framework, so that the acidity and Si/Al ratio are changed [28]. In general, dealumination can be carried out by using steam, acid, or heat treatment [29],[30],[31],[32]. Besides those advantages, the use of dealumination techniques have some disadvantages. First, a partial amorphization of the zeolite occurs, in which it results in the relative crystallinity to drop [28]. After that, the formed cavities and mesopores are often not connected or located in the zeolite framework, in which they are not connected to the surface, so that it is not really optimal to accelerate the molecule transport in the crystal [28]. Furthermore, the pore size distribution of the obtained mesopores is wide [29],[33],[30],[34].

2. Desilication

Desilication is occurred when contacting the zeolite with an alkaline solution, like it is diluted by NaOH, so that Si – O – Si bonds are selectively hydrolyzed resulting in the preferable removal of Si from the zeolite framework, and then the mesopores formed [33],[32],[31]. The initial process is preferably occurred at the boundaries of the zeolite crystal or at the structural defects [28]. Therefore, the crystal morphology of zeolite has a huge influence on the desilication process [35],[32],[36]. Furthermore, Al in the framework has an important role during desilication (i.e. framework Si/Al ratio), in which the charge of framework Al prevents the extraction of nearby Si species [29],[33],[30],[34]. Figure 1.12 shows an illustration of Al content influence on MFI zeolite desilication in NaOH.

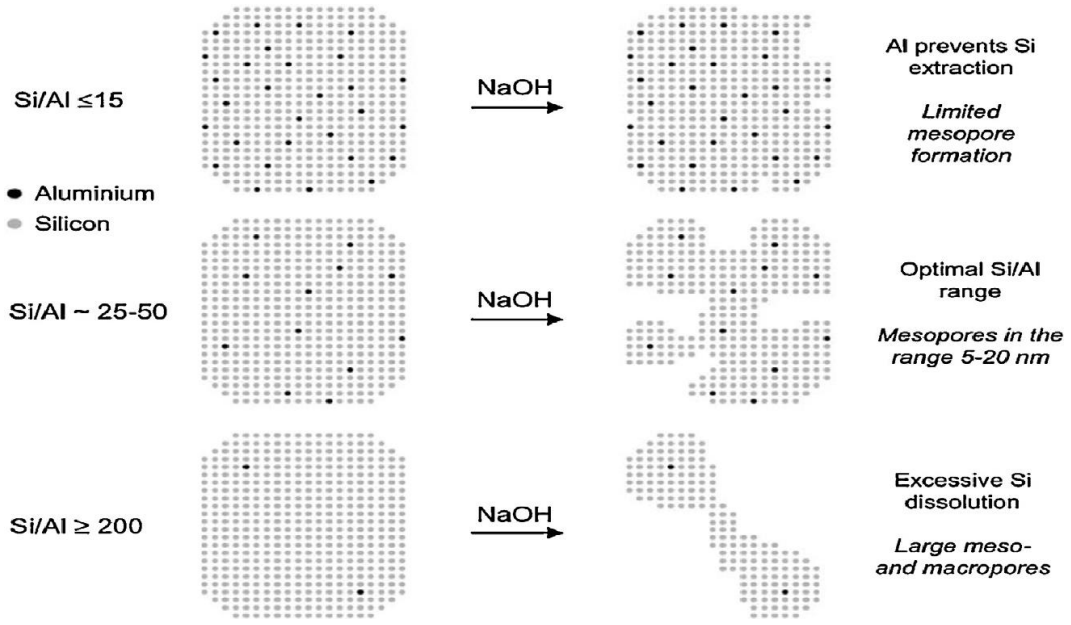

Figure 1.12. An illustration of Al content influence on MFI zeolite desilication in NaOH solution and the associated mechanism for pore formation [37].

Unfortunately, when the desilication process occurs, the interconnected mesopores are able to be formed while zeolite (largely) keeps its microporous character [28]. However, when the used concentration of alkaline solutions is too high, a lot of zeolite material is able to be lost and the microporosity could decline dramatically [31],[32]. Furthermore, it is difficult to produce abundant mesopores in large zeolite crystals [29],[30].

3. Dissolution-recrystallization

This technique is based on the recrystallization of a partially dissolved zeolite. The method composed of two main steps, i.e., 1) a part of the zeolite is dissolved (usually in the alkaline solution); then, 2) it is recrystallized by reassembling the dissolved and dispersed species to become a mesoporous structure [28]. This recrystallization carried out during a hydrothermal process in the presence of a surfactant. Level of dissolution and recrystallization are very influence towards the types of the hierarchical zeolite that can be formed as shown in Figure 1.13.

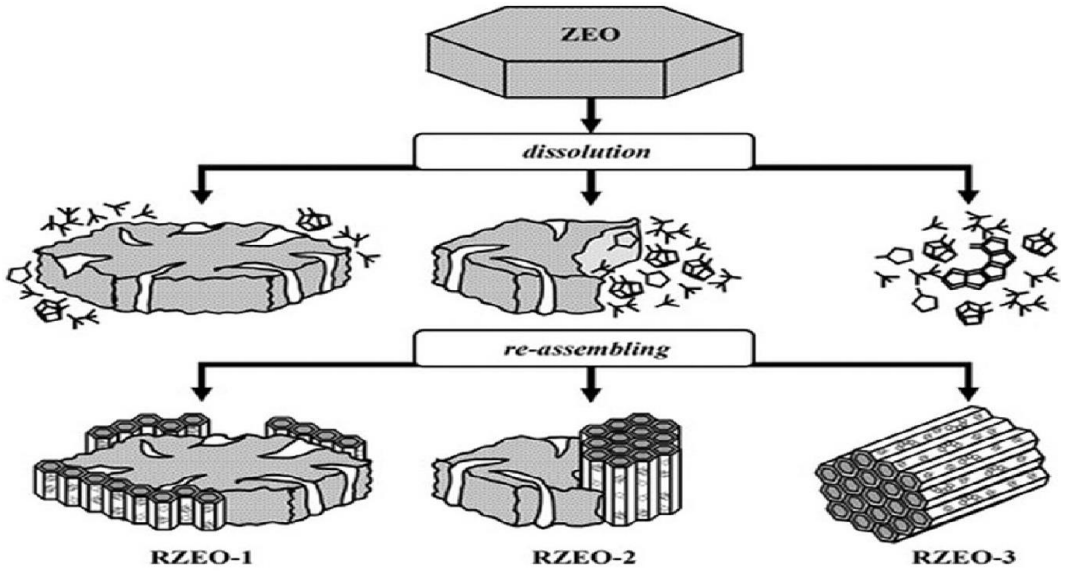

Figure 1.13. Illustration of the recrystallization process leading to different types of material [38].

RZEO – 1 has the same zeolitic phase as the parent material and is covered by a thin film of a mesoporous phase. RZEO – 2 is a composite material comprising of both a zeolitic and a mesoporous phase, in which the mesoporous phase be able to be an amorphous or regular (usually MCM-41) [28]. Whereas RZEO – 3 is a material which has been completely recrystallized and only has a mesoporous structure, usually MCM-41 [38].

1.2.2. Bottom-up methods

This method, in principle, produces the mesopore during the synthesis of the zeolite. Mesoporogen is often used to produce the mesopores, but template-free method also exists. There are three approaches that usually used via this method; 1) hard templating, 2) soft templating, and 3) template free.

1. Hard templating

This approach involves using a solid material with a relatively rigid structure as carbon materials, polymers and biological materials [28]. When they are used in the zeolite synthesis, they will act as a template which is surrounded by the microporous structure is being

synthesized. After the synthesis finishes, they is removed by calcination or dissolution to produce meso- or macropores [29],[33],[30],[31],[32]. Unfortunately, hard templates need high temperatures when they used and have hydrophobic character, so that their applications are limited and often occurred separation between mesoporous structure and microporous structure [29],[30],[32],[39]. Therefore, the hierarchical zeolite which synthesized using hard templates are often hydrothermally and mechanically less stable [28].

2. Soft templating

In principle, this approach involves the usage of two templates during the process of zeolite synthesis. First, it is a Structural Directing Agent (SDA) which is responsible to form the micropore in the zeolite, whereas the second one is a mesoporogen which is responsible for the formation of mesopore [28]. Mesoporogens are usually used as a soft template, i.e., surfactants, polymers, or organosilanes [29],[30],[32],[39],[40]. These soft templates are not only forming the mesopore but also they can interact chemically with the formed zeolite phase [32], so that they can be considered as a physical scaffold [28]. Interestingly, they can be tailored so that the size of mesoporous can be easily adjusted [32],[39],[40]. However, there are several things needing to be concerned, like the amorphous mesoporous material is possible be generated instead of crystalline hierarchical zeolites and defect sites can be formed during synthesis, in which they will result in the hydrothermal stability of zeolite becoming lower [28]. Because this approach uses two templates together, then it is often called as a dual-template method as well.

3. Template free

This approach does not need a mesoporogen to form the hierarchical zeolites. The synthesis method becomes a key to produce the hierarchical structure, in which a seed-assisted synthesis is a possible route [28]. These seeds are small proto-zeolitic units from early stages of zeolite crystallization and they are able to be added to a synthesis gel [28]. By addition them,

the obtained crystallinity can be increased and mesoporosity can be set [28]. Unfortunately, the mechanism of this synthesis is not fully understood. Furthermore, the technique of seed-assisted synthesis is also possible to combine with SDA [29],[30].

1.2.3. The mixed method

This method involves formation of nanozeolites and their assembly. Nanozeolites are defined as zeolite crystal with the crystal size in the nanometer range [28]. Because they have a small size, so that they have a high external surface area, short diffusion path, a high external/internal atom number ratio, and a high number of accessible active sites [33],[32],[39]. Consequence of these properties, nanozeolites exhibit a higher performance, an increased activity and a longer lifetime in catalytic applications [39]. Formation of nanozeolites can be achieved by several ways, such as with or without the use of SDAs, seed-induced, through milling and recrystallization, via confining the space growth, by using microwaves or ultrasonic irradiation, or by controlling the kinetics of the nucleation and crystal growth [32],[39],[41],[42].

After nanozeolites produced, they are assembled into larger ordered structures, and then the hierarchical structure is obtained that contains inter(nano)crystalline mesopores [28]. The mesopores are able to be set by the size of the nanocrystals. Consequence from this structure, it exhibits the improved properties compared to the conventional zeolites due to fusing the superior properties of nanozeolites as having been explained above and the presence of the mesopores which is able to be faster the mass transport in and out the zeolite system [28],[33],[32],[40].

1.3. ZSM-5 zeolite

ZSM-5 zeolite has MFI framework that constructed from 5-rings and contains a straight 10-ring channel system and a sinusoidal 10-ring channel system (Figure 1.14). In addition,

ZSM-5 has a chemical formula of $|Na_n^+(H_2O)_{16}|[Al_nSi_{96-n}O_{192}]$, n < 27 and space group of orthorhombic [43],[14],[44]. The O – T – O bond angles vary between 105^0 and 113^0 with an average value of 109 ± 2^0 [2]. The tetrapropylammonium ion (TPA^+), typically used for synthesizing the MFI framework which is located in the channel intersection of the sinusoidal and straight channels, with a different conformation from that in TPABr [45].

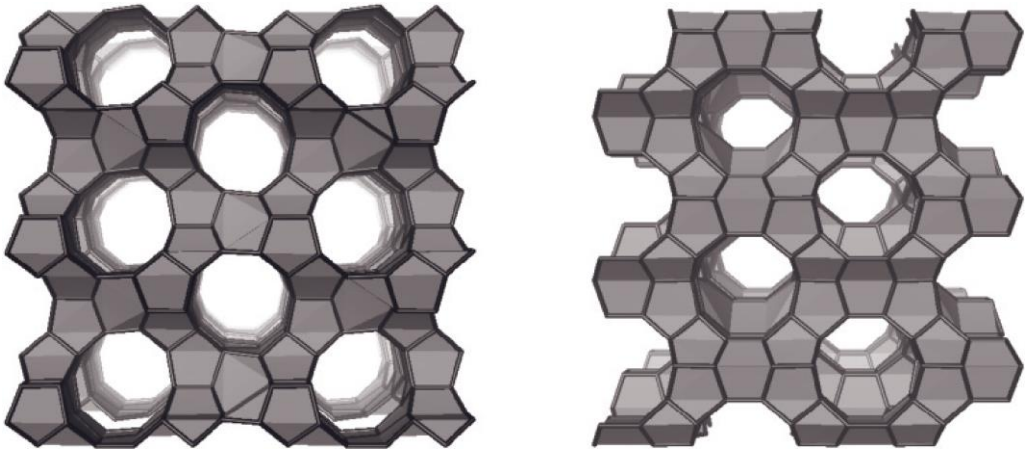

Figure 1.14. MFI framework views: (left) down the straight 10-ring channel system, (right) down the sinusoidal 10-ring channel system [1].

ZSM-5 is categorized as high silica zeolite (Si/Al ratio of 10-100 or higher [14]), so that it has the moderate hydrophilic property to highly hydrophobic property. Although the Al content is low, but the acidity that manifested by this zeolite is still sufficient for hydrocarbon catalysis reactions. ZSM-5 has highly thermal stability (>1000 ^oC) and acidic stability (up to pH of 3), so that it allows ZSM-5 to exchange cations to hydrogen ions directly without much Al loss [46].

1.4. Cracking

Cracking is one of the important processes in the petrochemical industry as it cleaves the heavy petroleum faction into smaller compounds, like alkanes (paraffins) and alkenes which are more useful. Among several cracking processes have been implemented in the

petrochemical industry, fluid catalytic cracking (FCC) which is a catalytic process using an acidic zeolite catalyst is the most used process since it does not require a very high temperature like the steam cracking process and is easier to be scaled-up the production capacity. Because the core of this process is the catalyst, then the catalyst is the key point for FCC.

Besides cracking of heavy petroleum fraction on acidic zeolite catalysts is one of the most important commercial processes, this reaction has been also used frequently to characterize the catalytic activity. For H-type of zeolites, the cracking rate of hydrocarbons were often found increase linearly with the framework aluminum content that corresponds to the density of brønsted acid sites [13]. For example, on H-ZSM-5 and H-Y zeolites, over a wide range of framework compositions, the rate of *n*-hexane cracking with aluminum content experiences a linear increase [47],[48],[49],[50]. Interestingly, when mild steaming applied, a significant increase in the *n*-hexane cracking rate in comparison with non-steamed H-ZSM-5 zeolites with equal brønsted acid site densities was observed [25]. This improved activity was attributed to superacidic brønsted sites obtained by a synergism of lewis sites at around bridging OH groups. Moreover, the cracking rates may also depend on the zeolite structure, even for non-steamed catalysts [51]. These examples illustrate that taking conclusion on the density of brønsted acid sites based on results of cracking reactions needs a caution.

On the catalytic test of H-type zeolite via *n*-hexane cracking, there are two possible mechanisms which are occurred. First, it is a mechanism of thermal cracking. Second, it is mechanism of catalytic cracking. For the mechanism of thermal cracking, it experiences the chain cracking (bond scission) processes involving the formation of carbenium ion intermediates, and their subsequent reactions involve carbenium ion rearrangement, β-bond scission and hydride transfer or hydrogenation [52] At the cracking temperature, thermal cleavage of carbon – carbon bonds occur readily.

$$CH_3CH_2CH_2CH_2CH_2CH_3 \longrightarrow CH_3CH_2CH_2\cdot + \cdot CH_2CH_2CH_3$$

It provides the initiation step for a free radical chain reaction. Then, the formed radicals undergo a series of β-scission reactions, each producing a molecule of ethylene.

$$CH_3CH_2CH_2\cdot \longrightarrow CH_3\cdot + CH_2{=}CH_2$$

Hydrogen atom abstraction from a substrate molecule by a methyl radical continues the reaction chain.

$$CH_3\cdot + C_6H_{14} \longrightarrow CH_4 + C_6H_{13}\cdot$$

Most substrate molecules are involved in the reaction via hydrogen atom abstraction rather than carbon – carbon cleavage. For both energetic and statistical reasons, then the formed radicals will be predominantly secondary radicals, and while these radicals undergo β-scission, alkenes other than ethylene will be produced.

$$CH_3CH_2CH_2CH_2CH{\cdot}CH_3 \longrightarrow CH_3CH_2CH_2\cdot + CH_2{=}CHCH_3$$

Then, the produced primary radicals can experience further β-scission that produce ethylene.

$$CH_3CH_2CH_2\cdot \longrightarrow CH_3\cdot + CH_2{=}CH_2$$

On the other hand, the mechanism of catalytic cracking involves classic cracking mechanism (bimolecular) and monomolecular cracking mechanism. The bimolecular cracking is believed to be initiated via intermolecular hydride transfer (HT) from alkanes to smaller carbenium ions that are formed by protonation of light alkenes present in the feed in trace quantities or made via thermal reactions [1]. Then, the formed carbenium ions undergo β-scission to form the light alkenes and the small carbenium ions [53]. Therefore, *n*-hexane cracking via the bimolecular cracking mechanism can be illustrated as follows [54],[55].

$$C_3H_{14} + C_3H_7{}^+Z^- \xrightarrow[\beta\text{-scission}]{HT} C_6H_{13}{}^+Z^- + C_3H_8 \qquad (1)$$

Z = zeolite

$$C_6H_{13}^{+}Z^{-} \longrightarrow C_3H_7^{+}Z^{-} + C_3H_6 \quad (2)$$

This mechanism is predominant occurred at low reaction temperature, high alkane partial pressure, high conversions, wide space of reaction, and high Al content of zeolites [56],[54]. Hydrocarbons with the number of carbons of two are rarely produced by this mechanism since these products need the primary carbenium ions which are energetically unfavorable to form them [56],[55],[57]. Therefore, the formation of propylene and butenes is easier compared to ethylene formation.

While on the monomolecular cracking mechanism, it is initiated by direct protonation over brønsted acid sites to produce a carbonium ion and do not involve assistance from another molecule [1]. For the formation of light paraffins from *n*-hexane via the monomolecular cracking mechanism can be accounted for by a simple cleavage of a penta-coordinated carbonium ion ($C_6H_{15}^{+}$) into a smaller alkane (C_nH_{2n+2}) and a classical carbenium ion ($C_mH_{2m+1}^{+}$) with $n + m = 6$. After that, the formed carbenium ions are transformed to alkenes by desorption or β-scission step. This mechanism can be illustrated as follows [56].

$$C_6H_{14} + H\text{-}Z \longrightarrow C_6H_{15}^{+}Z^{-} \longrightarrow C_{(6-n)}H_{2(6-n)+2} + C_mH_{2m+1}^{+}Z^{-} \quad (1)$$

Z = zeolite

$$C_mH_{2m+1}^{+}Z^{-} \xrightarrow[\text{desorption}]{\beta\text{-scission}} C_mH_{2m} + H\text{-}Z \quad (2)$$

Because hydrogen is also observed by this mechanism, so that the reaction probably be like this [56].

$$C_6H_{14} + H\text{-}Z \longrightarrow C_6H_{15}^{+}Z^{-} \longrightarrow C_6H_{13}^{+}Z^{-} + H_2 \quad (3)$$

Meanwhile, for 3-methylpentane cracking (the branched isomer of n-hexane), it can be illustrated as shown by Figure 1.15.

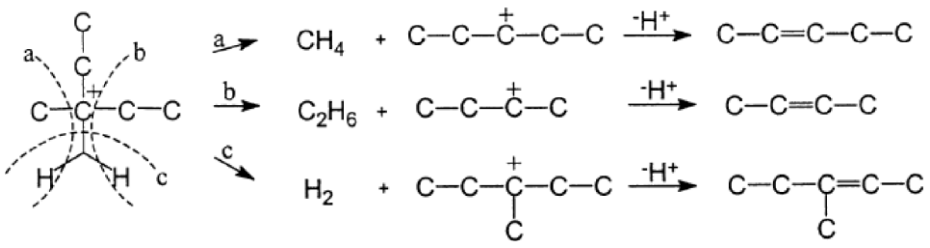

Figure 1.15. Preferential protonation and collapse of a 3-methylpentane molecule [55].

This mechanism is predominant occurred at high reaction temperature, low alkane partial pressure, low conversion, narrow space of reaction and low Al content of zeolite [56],[54]. Meanwhile, the product distribution will be similar to that obtained via a radical cracking mechanism, i.e., larger H_2, CH_4, and C_2 [55].

1.5. Methanol to olefins

Methanol to olefins (MTO) reaction is one of the most important reactions in the petrochemical industry for providing basic petrochemicals other than involving oil routes. MTO is believed becoming a linkage between an old petrochemical industry and a modern petrochemical industry due to the whole process is new and cheap, and the feedstock, methanol, is different from the conventional feedstocks which are derived from fossil resources, i.e., naphtha, liquid pressurized gas (LPG), or ethane [58].

MTO is an autocatalytic reaction, in which the initial formation of a small amount of products forces toward an increased methanol conversion until the efficient production period reached [59],[60]. In the methanol to olefins process, the formation of the first C-C bond is the limiting step in the kinetic of methanol to hydrocarbons. Therefore, many early studies proposed mechanisms of C-C bond formation, such as carbene mechanism [61],[62], oxonium ylide mechanism [63],[64], free radical mechanism [65],[66], carbocationic mechanism [60],[66], and so on. However, they are proved later energetically unfavorable by the theoretical calculation [67]. At present, the hydrocarbon pool (HCP) mechanism and the "dual-

cycle" concept are well accepted for MTO reaction as they allow the best fitting between the theoretical calculations and the experimental data [68]. Briefly, in the olefinic hydrocarbon pool (first concept), the higher olefins formed by the methylation of light olefins (worked as reactive species), and then they cracked into propene and butenes. In the aromatic hydrocarbon pool (second concept), methylated benzenes acted as active intermediates to produce olefins, in which methylbenzenes with two or three methyl groups primarily produce ethene, whereas the higher metylbenzenes prefer to produce propene and butenes [69]. Those cycles work parallel and compete with each other.

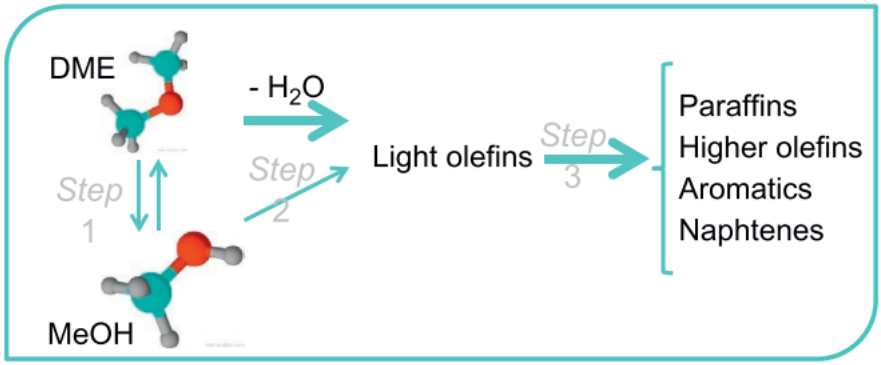

Figure 1.16. Reaction steps of methanol (MeOH) conversion into hydrocarbons [70].

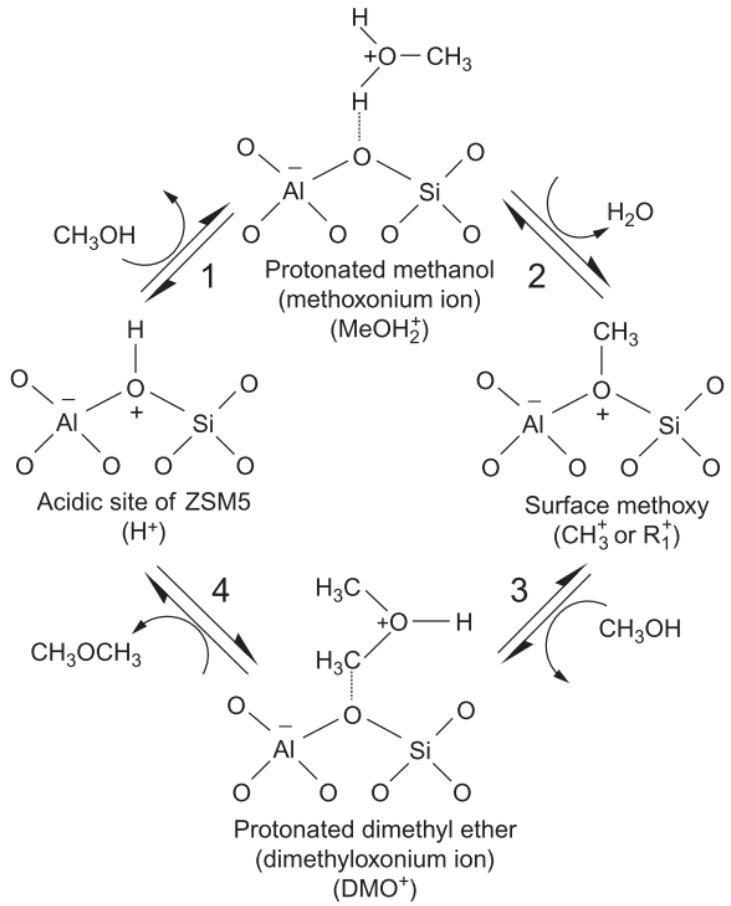

Figure 1.17. The reaction mechanism for the formation of DME by dehydration of methanol over H-ZSM-5 catalyst [71], [72], [73].

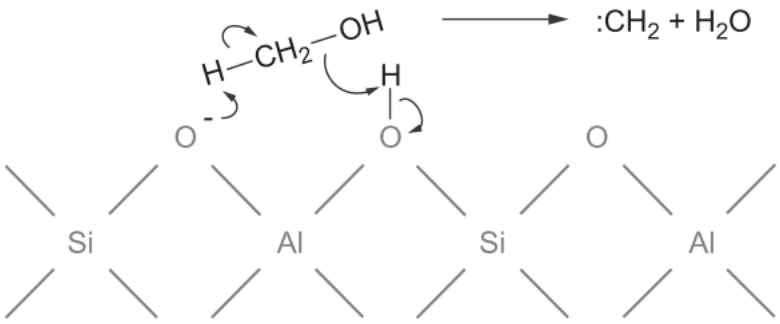

Figure 1.18. The possible mechanism for carbene formation on the zeolite surface [60].

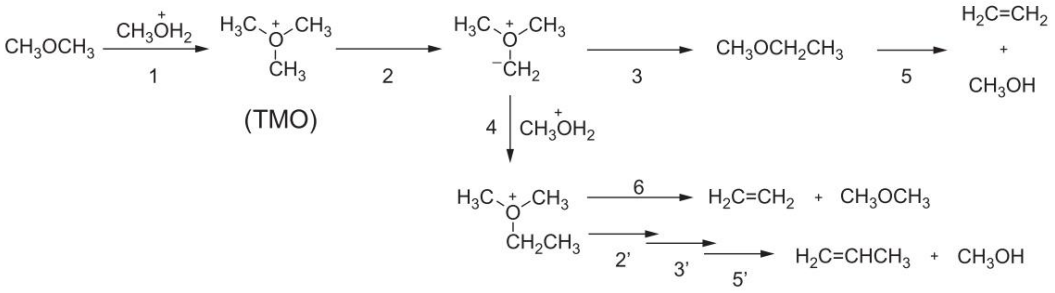

Figure 1.19. Oxonium ylide mechanism [74].

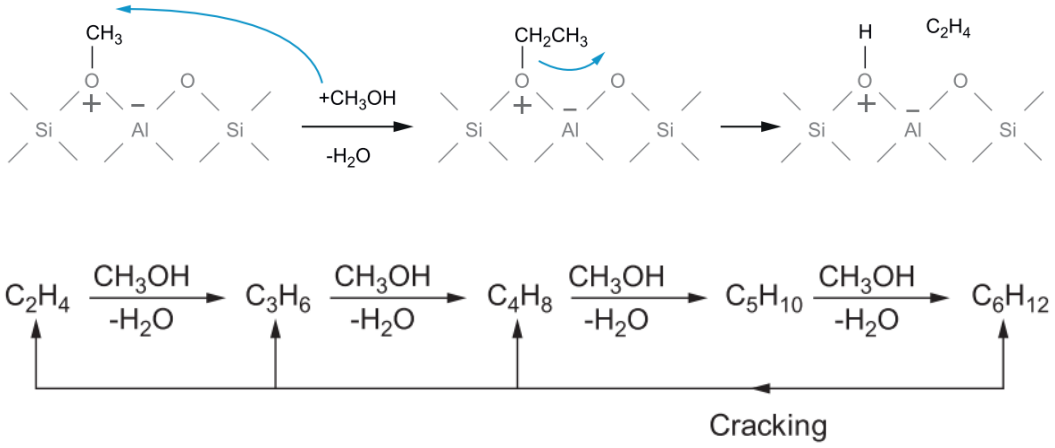

Figure 1.20. Surface methoxy mechanism and scheme of rake mechanism in the carbocationic mechanism (the surface methoxy mechanism) [75], [76].

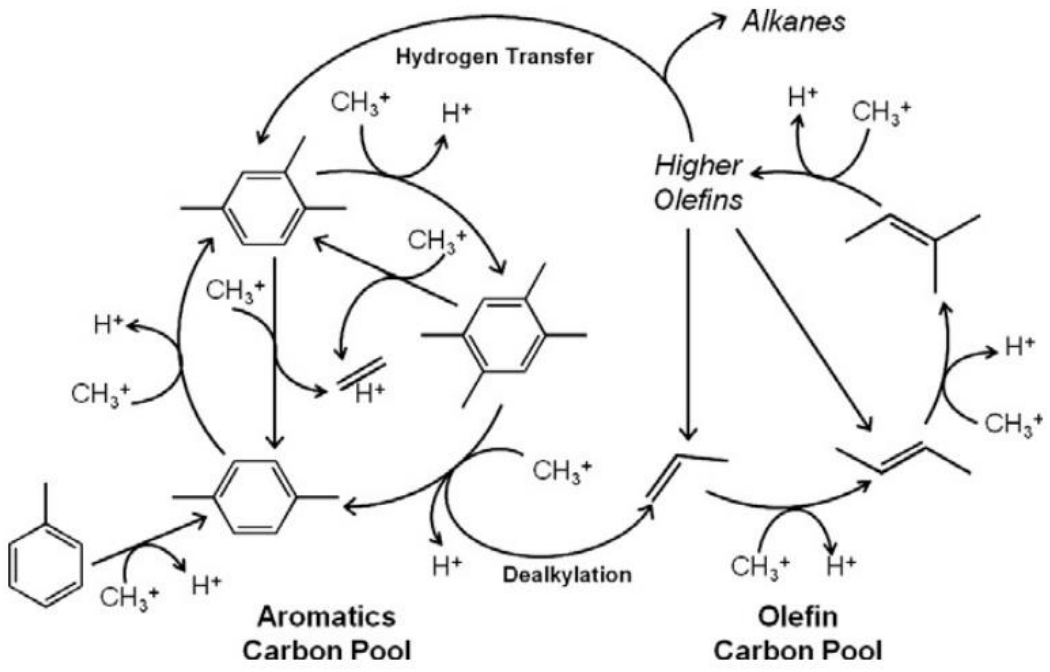

Figure 1.21. The suggested dual-cycle concept for methanol conversion over ZSM-5 zeolite [77].

1.6. Objects and outline of this thesis

The object of this study is to modify the framework structure (microporous structure) to be the hierarchical structure and modify the aluminum distribution in the framework of the hierarchical structure, with the final objective of enhancing the selectivity in the catalytic process. To deeply understand the changes in aluminum distribution and the framework structure on the hierarchical ZSM-5, the synthesis conditions and composition of the starting material are varied. The impact of its aluminum distribution and modified structure on the catalytic performance is studied as well. This thesis consists of four chapters, in which the first chapter is the general introduction (this chapter).

The second chapter focused on the synthesis of the hierarchical ZSM-5 intracrystalline with the controlled aluminum distribution. To synthesize the hierarchical ZSM-5 intracrystalline, a bottom-up approach using a surfactant as mesoporogen is used. the aluminum

distribution on the synthesized hierarchical ZSM-5 intracrystalline. Whereas to control the aluminum distribution, the addition of sodium or without the addition of sodium into the synthetic gel is carried out. Furthermore, the impact of the aluminum distribution and the modified structure obtained from those treatments on the catalytic processes is observed as well. The reaction of *n*-hexane cracking and methanol conversion is applied to determine those effects.

The third chapter discusses the effect of the synthesis condition and composition of the starting material on the aluminum distribution and the formed hierarchical structure over the hierarchical ZSM-5 intracrystalline. The parameters of the synthesis condition being applied in this Chapter are the crystallization temperature, the pH of the synthetic gel, and the timing of mesoporogen addition into the synthetic gel. While, for the parameter of the composition of the starting material, the mesoporogen concentration is applied. On the other hand, the reaction of methanol conversion is carried out as the catalytic evaluation and investigator of Al distribution.

The fourth chapter is a summary of this dissertation and the future prospects of this study.

1.7. Reference

[1] S. Kulprathipanja, Zeolites in Industrial Separation and Catalysis, 2010.

[2] S.M. Auerba, Zeolite Science and perspectives, 2003.

[3] D.M. Ruthven, M.F.M. Post, Diffusion in zeolite molecular sieves, Stud. Surf. Sci. Catal. 137 (2001) 525–577.

[4] H. van Koningsveld, J.C. Jansen, H. van Bekkum, The monoclinic framework structure of zeolite H-ZSM-5. Comparison with the orthorhombic framework of as-synthesized ZSM-5, Zeolites. 10 (1990) 235–242.

[5] S.M. Csicsery, Sigmund M. Csicsery, Shape-selective catalysis in zeolites, Zeolites. 4 (1984) 116–126.

[6] W.H. Baur, Straight Si–O–Si bridging bonds do exist in silicates and silicon dioxide polymorphs, Acta Crystallogr. Sect. B Struct. Crystallogr. Cryst. Chem. 36 (1980) 2198–2202.

[7] W.H. Baur, D. Kassner, C.-H. Kim, N.H.W. Sieber, Flexibility and distortion of the framework of natrolite: crystal structures of ion-exchanged natrolites, Eur. J. Mineral. 2 (1990) 761–770.

[8] E. Stuckenschmidt, W. Joswig, W.H. Baur, Flexibility and distortion of the collapsible framework of NAT topology: the crystal structure of H3O-natrolite, Eur. J. Mineral. 8 (1996) 85–92.

[9] I. Petrovic, A. Navrotsky, M.E. Davis, S.I. Zones, Thermochemical Study of the Stability of Frameworks in High Silica Zeolites, Chem. Mater. 5 (1993) 1805–1813.

[10] P.M. Piccione, C. Laberty, S. Yang, M.A. Camblor, A. Navrotsky, M.E. Davis, Thermochemistry of Pure-Silica Zeolites, (2000) 10001–10011.

[11] Mobil Oil, J. Catal. 312 (1962) 307–312.

[12] P. B. Weiz, V.J. Frilette, J. Phys. Chem. 64 (1960), 382.

[13] J. Čejka, A. Corma, S. Zones, Zeolites and Catalysis: Synthesis, Reactions and Applications, 2010.

[14] W.L. Bragg, Crystal structure, Nature. 105 (1920) 646–648.

[15] S.M. Csicsery, Shape-selective catalysis in zeolites, Zeolites. 4 (1984) 202–213.

[16] W.O. Haag, R.M. Lago, P.B. Weisz, Transport and reactivity of hydrocarbon molecules in a shape-selective zeolite, Faraday Discuss. Chem. Soc. 72 (1981) 317–330.

[17] S.I. Zones, T. V. Harris, The Constraint Index test revisited: Anomalies based upon new zeolite structure types, Microporous Mesoporous Mater. 35–36 (2000) 31–46.

[18] T.F. Degnan, The implications of the fundamentals of shape selectivity for the development of catalysts for the petroleum and petrochemical industries, J. Catal. 216 (2003) 32–46.

[19] M. Elanany, M. Koyama, M. Kubo, E. Broclawik, A. Miyamoto, Periodic density functional investigation of Lewis acid sites in zeolites: Relative strength order as revealed from NH 3 adsorption, Appl. Surf. Sci. 246 (2005) 96–101.

[20] M. Hunger, U. Schenk, M. Breuninger, R. Gläser, J. Weitkamp, Characterization of the acid sites in MCM-41-type materials by spectroscopic and catalytic techniques, Microporous Mesoporous Mater. 27 (1999) 261–271.

[21] W. Hu, Q. Luo, Y. Su, L. Chen, Y. Yue, C. Ye, F. Deng, Acid sites in mesoporous Al-SBA-15 material as revealed by solid-state NMR spectroscopy, Microporous Mesoporous Mater. 92 (2006) 22–30.

[22] X. Xie, M. Satozawa, K. Kunimori, S. Hayashi, NMR study of pore surface and size in the mesoporous material FSM-16, Microporous Mesoporous Mater. 39 (2000) 25–35.

[23] A. Corma, State of the art and future challenges of zeolites as catalysts, J. Catal. 216 (2003) 298–312.

[24] R.A. Shigeishi, B.H. Chiche, F. Fajula, CO adsorption on superacid sites on dealuminated mazzite, Microporous Mesoporous Mater. 43 (2001) 211–226.

[25] R.M. Lago, W.O. Haag, R.J. Mikovsky, D.H. Olson, S.D. Hellring, K.D. Schmitt, G.T. Kerr, The nature of the catalytic sites in HZSM-5 - Activity enhancement, Stud. Surf. Sci. Catal. 28 (1986) 677–684.

[26] E. Brunner, H. Ernst, D. Freude, M. Hunger, C.B. Krause, D. Prager, W. Reschetilowski, W. Schwieger, K.H. Bergk, Solid-state n.m.r. and catalytic studies of mildly hydrothermally dealuminated HZSM-5, Zeolites. 9 (1989) 282–286.

[27] K. Zhang, M.L. Ostraat, Innovations in hierarchical zeolite synthesis, Catal. Today. 264 (2016) 3–15.

[28] D. Kerstens, B. Smeyers, J. Van Waeyenberg, Q. Zhang, J. Yu, B.F. Sels, State of the Art and Perspectives of Hierarchical Zeolites: Practical Overview of Synthesis Methods and Use in Catalysis, Adv. Mater. 32 (2020) 1–47.

[29] R. Bai, Y. Song, Y. Li, J. Yu, Creating Hierarchical Pores in Zeolite Catalysts, Trends Chem. 1 (2019) 601–611.

[30] X. Jia, W. Khan, Z. Wu, J. Choi, A.C.K. Yip, Modern synthesis strategies for hierarchical zeolites: Bottom-up versus top-down strategies, Adv. Powder Technol. 30 (2019) 467–484.

[31] K. Li, J. Valla, J. Garcia-Martinez, Realizing the commercial potential of hierarchical

zeolites: New opportunities in catalytic cracking, ChemCatChem. 6 (2014) 46–66.

[32] K. Möller, T. Bein, Mesoporosity – a new dimension for zeolites, Chem. Soc. Rev. 42 (2013) 3689–3707.

[33] A. Feliczak-Guzik, Hierarchical zeolites: Synthesis and catalytic properties, Microporous Mesoporous Mater. 259 (2018) 33–45.

[34] S. Van Donk, A.H. Janssen, J.H. Bitter, K.P. De Jong, Generation, characterization, and impact of mesopores in zeolite catalysts, Catal. Rev. - Sci. Eng. 45 (2003) 297–319.

[35] D. Verboekend, J. Pérez-Ramírez, Design of hierarchical zeolite catalysts by desilication, Catal. Sci. Technol. 1 (2011) 879–890.

[36] R. Chal, C. Gérardin, M. Bulut, S. VanDonk, Overview and Industrial Assessment of Synthesis Strategies towards Zeolites with Mesopores, ChemCatChem. 3 (2011) 67–81.

[37] J.C. Groen, J.C. Jansen, J.A. Moulijn, J. Pérez-Ramírez, Optimal aluminum-assisted mesoporosity development in MFI zeolites by desilication, J. Phys. Chem. B. 108 (2004) 13062–13065.

[38] I.I. Ivanova, E.E. Knyazeva, Micro-mesoporous materials obtained by zeolite recrystallization: Synthesis, characterization and catalytic applications, Chem. Soc. Rev. 42 (2013) 3671–3688.

[39] E. Koohsaryan, M. Anbia, Nanosized and hierarchical zeolites: A short review, Cuihua Xuebao/Chinese J. Catal. 37 (2016) 447–467.

[40] V. Valtchev, S. Mintova, Hierarchical zeolites, MRS Bull. 41 (2016) 689–693.

[41] Q. Li, D. Creaser, J. Sterte, An investigation of the nucleation/crystallization kinetics of nanosized colloidal faujasite zeolites, Chem. Mater. 14 (2002) 1319–1324.

[42] S. Mintova, J.P. Gilson, V. Valtchev, Advances in nanosized zeolites, Nanoscale. 5 (2013) 6693–6703.

[43] L.N. Large, Ion Bombardment of Solids, Electron. Power. 14 (1968) 410.

[44] H. Van Koningsveld, H. Van Bekkum, J.C. Jansen, On the location and disorder of the tetrapropylammonium (TPA) ion in zeolite ZSM-5 with improved framework accuracy, Acta Crystallogr. Sect. B. 43 (1987) 127–132.

[45] K.J. Chao, J.C. Lin, Y. Wang, G.H. Lee, Single crystal structure refinement of TPA ZSM-5 zeolite, Zeolites. 6 (1986) 35–38.

[46] F.J. van der Gaag, ZSM-5 type zeolites :Synthesis and use in gasphase reactions with ammonia, (1987) 1–132.

[47] D.H. Olson, W.O. Haag, R.M. Lago, Chemical and physical properties of the ZSM-5 substitutional series, J. Catal. 61 (1980) 390–396.

[48] W.O. Haag, R.M. Lago, P.B. Weisz, The active site of acidic aluminosilicate catalysts, Nature. 309 (1984) 589–591.

[49] S.J. DeCanio, J.R. Sohn, P.O. Fritz, J.H. Lunsford, Acid catalysis by dealuminated zeolite-Y. I. Methanol dehydration and cumene dealkylation, J. Catal. 101 (1986) 132–141.

[50] J.N. Miale, N.Y. Chen, P.B. Weisz, Catalysis by crystalline aluminosilicates. IV. Attainable catalytic cracking rate constants, and superactivity, J. Catal. 6 (1966) 278–287.

[51] E.G. Derouane, C.D. Chang, Confinement effects in the adsorption of simple bases by zeolites, Microporous Mesoporous Mater. 35–36 (2000) 425–433.

[52] P. Wiseman, Ethylene by naphtha cracking free radicals in action, J. Chem. Educ. 54 (1977) 154–156.

[53] C.L. Thomas, Chemistry of Cracking Catalysts, Ind. Eng. Chem. 41 (1949) 2564–2573.

[54] W.O. Haag, R.M. Dessau, R.M. Lago, Kinetics and Mechanism of Paraffin Cracking with Zeolite Catalysts, Stud. Surf. Sci. Catal. 60 (1991) 255–265.

[55] S. Kotrel, H. Knözinger, B.C. Gates, The Haag-Dessau mechanism of protolytic cracking of alkanes, Microporous Mesoporous Mater. 35–36 (2000) 11–20.

[56] A.F.H. Wielers, M. Vaarkamp, M.F.M. Post, Relation between properties and performance of zeolites in paraffin cracking, J. Catal. 127 (1991) 51–66.

[57] A. Corma, A. V Orchille, Current views on the mechanism of catalytic cracking, Micropor. Mesopor. Mater. 35-36 (2000) 21-30.

[58] W. Vermeiren, J.P. Gilson, Impact of zeolites on the petroleum and petrochemical industry, Top. Catal. 52 (2009) 1131–1161.

[59] N.Y. Chen, W.J. Reagan, Evidence of autocatalysis in methanol to hydrocarbon reactions over zeolite catalysts, J. Catal. 59 (1979) 123–129.

[60] Y. Ono, T. Mori, Mechanism of methanol conversion into hydrocarbons over ZSM-5 zeolite, J. Chem. Soc. Faraday Trans. 1 Phys. Chem. Condens. Phases. 77 (1981) 2209–2221.

[61] C.D. Chang, A.J. Silvestri, The conversion of methanol and other O-compounds to hydrocarbons over zeolite catalysts, J. Catal. 47 (1977) 249–259.

[62] C.D. Chang, C.T.W. Chu, On the mechanism of hydrocarbon formation from methanol over zeolite catalysts: Evidence for carbene intermediacy, J. Catal. 74 (1982) 203–206.

[63] G.A. Olah, Appi. Chem., Vol.53, pp.201—207. Pergamon Press Ltd. 1981. Printed in Great Britain. HIGHER COORDINATE (HYPERCARBON CONTAINING) CARBOCATIONS AND, 53 (1981) 201–207.

[64] G.J. Hutchings, F. Gottschalk, M.V.M. Hall, R. Hunter, Hydrocarbon formation from methylating agents over the zeolite catalyst ZSM-5., J. Chem. Soc. Faraday Trans. 1. 83 (1987) 571.

[65] J.K.A. Clarke, R. Darcy, B.F. Hegarty, E. O'Donoghue, V. Amir-Ebrahimi, J.J. Rooney, Free radicals in dimethyl ether on H-ZSM-5 zeolite. A novel dimension of heterogeneous catalysis, J. Chem. Soc. Chem. Commun. (1986) 425–426.

[66] M. Stöcker, Methanol-to-hydrocarbons: Catalytic materials and their behavior, Microporous Mesoporous Mater. 29 (1999) 3–48.

[67] P. Tian, Y. Wei, M. Ye, Z. Liu, Methanol to olefins (MTO): From fundamentals to commercialization, ACS Catal. 5 (2015) 1922–1938.

[68] N. Nesterenko, J. Aguilhon, P. Bodart, D. Minoux, J.P. Dath, Methanol to Olefins: An Insight Into Reaction Pathways and Products Formation, 2016.

[69] U. Olsbye, S. Svelle, M. Bjrgen, P. Beato, T.V.W. Janssens, F. Joensen, S. Bordiga, K.P. Lillerud, Conversion of methanol to hydrocarbons: How zeolite cavity and pore size controls product selectivity, Angew. Chemie - Int. Ed. 51 (2012) 5810–5831.

[70] Chang, C D, and Silvestri, A J. 1987. "MTG: origin, evolution operation." United States.

[71] Park, TY, and Gilbert Froment. 2001. "Kinetic Modeling of the Methanol to Olefins Process, 1 : Model Formulation." *INDUSTRIAL & ENGINEERING CHEMISTRY RESEARCH* 40 (20): 4172–86.

[72] Park T-Y, Froment GF. Kinetic modeling of the methanol to olefins process. 2.

Experimental results, model discrimination, and parameter estimation. Ind Eng Chem Res 2001;40:4187–96.

[73] Park T-Y, Froment GF. Kinetic modeling of the methanol to olefins process. 1. Model formulation. Ind Eng Chem Res 2001;40:4172–86.

[74] Spivey JJ, Froment GF, Dehertog WJH, Marchi AJ. In: Spivey JJ, editor. Catalysis, vol. 9; 1992. p. 1–64.

[75] Stöcker M. Methanol-to-hydrocarbons: catalytic materials and their behavior. Microporous Mesoporous Mater 1999;29:3–48.

[76] Cormerais FX, Perot G, Chevalier F, Guisnet M. J Chem Res Synop 1980:362

[77] Ilias S, Bhan A. Mechanism of the catalytic conversion of methanol to hydrocarbons. ACS Catal 2013;3:18–31.

Chapter 2

Synthesis of hierarchical ZSM-5 intracrystalline with the controlled aluminum distribution

ABSTRACT

The hierarchical ZSM-5 intracrystalline with the adjusted aluminum distribution had been carried out. The hierarchical structure was synthesized by a bottom-up method using a surfactant (cetryltrimethylammonium bromide) as mesoporogen, while the adjustment of aluminum distribution was performed by adding or without adding sodium into the synthetic gel. It was found that the well-structured hierarchical ZSM-5 could be achieved by prolonging crystallization time for 144 h. Furthermore, this treatment resulted in an enhancement in the strength of acid sites and a change of crystal morphology from coffin-like morphology to flower-like morphology (the hierarchical ZSM-5 with Na) or coral reef-like morphology (the hierarchical ZSM-5 without Na). Meanwhile, for aluminum distribution, the hierarchical ZSM-5 containing Na gave rise to Al distribution more concentrated in the channel intersection than the hierarchical ZSM-5 without containing Na, which was a reversed trend compared to the original ZSM-5. The impact of those modifications on the reaction of *n*-hexane cracking and methanol conversion was also investigated. The hierarchical structure produced a higher selectivity in the production of lower olefins, especially propene, with the hierarchical ZSM-5 without Na being superior either in the reaction of *n*-hexane cracking or in the reaction of methanol conversion.

Chapter 3

The impact of synthesis conditions and mesoporogen concentration on the aluminum distribution in the hierarchical ZSM-5 intracrystalline

3.1. Introduction

In Chapter 2, we reported that aluminum distribution on the hierarchical ZSM-5 intracrystalline could be controlled by the addition of sodium or without sodium. Furthermore, crystallization time influenced not only the formed hierarchical structure but also the arrangement of aluminum in the framework. These findings indicated the synthesis condition influenced aluminum distribution as well.

In the zeolite catalyst field, adjustment of aluminum in the framework has been regarded as a major issue due to its position and distribution are considered to be important factors in both acidic and redox catalytic reactions. As reported by Wang [1] et.al., that the reaction pathway in the methanol-to-olefins (MTO) reaction could be varied by regulating of aluminum position in the framework, which was viewed via a comparison between ZSM-5 and ZSM-11. Meanwhile, recent studies have shown that the distribution of aluminum in the framework can be controlled by using various methods, such as the incorporation of heteroatoms [2],[3], the addition of the Structure-Directing Agent (SDA) [4],[5], and dealumination [6],[7]. Furthermore, Sungtak [8] et.al., reported that the aluminum distribution in the ZSM-5 framework could be controlled by adjusting the crystallization temperature. Those imply that the location of aluminum in the framework can be adjusted by the arrangement of synthesis conditions and composition of the starting materials.

By referring to my findings in Chapter 2 and the aforementioned findings, I investigate the relation of the synthesis conditions (crystallization temperature, the pH of the synthetic gel, and the timing of mesoporogen addition into the synthetic gel) and the composition of the starting materials (the mesoporogen concentration) toward the aluminum distribution in the hierarchical ZSM-5 intracrystalline in this work. For the evaluation of the distribution of aluminum in the pores, the methods used in this Chapter were the same as in Chapter 2, i.e., ^{27}Al MAS NMR and Co (II) ion UV-Vis DRS analyses. For the catalytic evaluation, the

methanol to olefins (MTO) reaction was carried out to investigate the effect of those treatments on the aluminum distribution.

3.2. Experiments

The synthesis procedures and the kind of characterizations used in this Chapter are, in principle, the same as in Chapter 2.

3.2.1. Synthesis

For the hierarchical samples with varying the crystallization temperature, the total molar ratio of the used gel is 64 Si_2O : 1 Al_2O_3 : 10 $TPA_2(O)$: 0.5 or 0 Na_2O : 4.4 CTAB : 3571 H_2O. Whereas for varying the mesoporogen concentration, the total molar ratio of gel is 64 Si_2O : 1 Al_2O_3 : 10 $TPA_2(O)$: 0.5 or 0 Na_2O : 2.2 CTAB : 3571 H_2O. All processes were carried out at room temperature and stirred condition. First, $Al(NO_3)_3.9H_2O$, NaOH, TPAOH, and TEOS were dissolved in demineralized water. Then, pH was adjusted to ~ 11 by the addition of acetic acid and continued by aging for 3 h. After that, CTAB was added into the mixture and continued by re-aging for 15 h. Subsequently, the obtained mixture was placed in the autoclave and followed by the crystallization process at **X** °C (**X** = 180 and 200 ^{0}C) for 144 h with the static condition, respectively. Afterward, the obtained suspension was filtered, washed with demineralized water, and dried overnight. Finally, the as-made hierarchical ZSM-5 was calcined at 550 °C for 5 h. The products were named as Hi_Z5_[TPA+Na]_**X_Y** and Hi_Z5_[TPA]_**X_Y** (**X** = for the crystallization temperature; **Y** = the mesoporogen concentration) for the hierarchical ZSM-5 containing sodium and without containing sodium, respectively.

To investigate the effect of the synthetic gel pH, first, $Al(NO_3)_3.9H_2O$, NaOH, TPAOH, and TEOS were dissolved in demineralized water. Second, aging the mixture for 3 hours without adjustment of pH. Then, CTAB was added into the mixture and continued by re-aging

for 15 h. The total molar ratio of gel: 64 Si_2O : 1 Al_2O_3 : 10 $TPA_2(O)$: 0.5 or 0 Na_2O : 4.4 CTAB : 3571 H_2O. After that, the mixture was placed in the autoclave and proceeded with the crystallization at 180 ^{0}C for 144 hours with the static condition. Subsequently, the suspension was filtered, washed with demineralized water, and dried. Afterward, the as-made hierarchical ZSM-5 was calcinated at 550 ^{0}C for 5 h. The product was named as Hi_Z5_[TPA+Na]_180_4.4_WApH and Hi_Z5_[TPA]_180_4.4_WApH. Whereas to investigate the impact of the timing of mesoporogen addition, the timing of TPAOH and CTAB addition was switched, with the pH of the mixture kept at ~ 11 and the total molar ratio of the used gel: 64 Si_2O : 1 Al_2O_3 : 10 $TPA_2(O)$: 0.5 or 0 Na_2O : 4.4 CTAB : 3571 H_2O. The next steps were the same. The product was labelled Hi_Z5_[TPA+Na]_180_4.4_Csw and Hi_Z5_[TPA]_180_4.4_Csw.

As a control, the typical microporous ZSM-5 samples with and without sodium were synthesized as references. The synthesis procedure was used similarly to the hierarchical procedure, in which the processes were performed at room temperature with the stirred condition and the total molar ratio of the gel: 64 SiO_2 : 1 Al_2O_3 : 10 TPA_2O : 0.5 or 0 Na_2O : 3571 H_2O. First, aluminum nitrate nonahydrate, sodium hydroxide, TPAOH, and TEOS were dissolved in demineralized water. After that, the aging was undertaken for 3 h. Subsequently, the crystallization process was performed at **X** °C (**X** = 180 and 200 ^{0}C) for 144 h with the rotating condition (40 rpm), respectively. The next synthesis procedure was the same as the hierarchical one. The obtained products were labeled as Mic_Z5_[TPA+Na]_**X** and Mic_Z5_[TPA]_**X** (**X** = the crystallization temperature) for the microporous ZSM-5 containing sodium and without containing sodium, respectively. H-type microporous ZSM-5 was achieved by the same ion exchange and calcination procedures as the hierarchical one.

For obtaining the H-type hierarchical ZSM-5, all samples were ion-exchanged twice by 1 M NH_4NO_3 aqueous solution at 80 °C for 3 h in the stirring condition, and then followed by

calcination at 550 °C for 4 h. Meanwhile, Co^{2+} ion-exchanged ZSM-5 zeolites were prepared by H-type ZSM-5 ion-exchanged back to Na-type ZSM-5 using 1 M $NaNO_3$ solution at 80 °C for 7 h. Then, Na-type ZSM-5 was ion-exchanged with 0.05 M $Co(NO)_3$ solution three times at 80 °C for 7 h. Finally, Co-ZSM-5 was obtained after being filtered, washed, and dried.

3.2.2. Characterization

The measurement conditions used in this Chapter followed as in Chapter 2. XRD patterns were acquired on a Rint-Ultima III (Rigaku) instrument using a Cu Kα X-ray source (40 kV, 40 mA for wide angle and 40 kV, 20 mA for small angle). For Field-Emission Scanning Electron Microscopic (FE-SEM) images, they were obtained on SU9000 (Hitachi) microscopes operated at 1 kV. The textural properties of the samples were calculated by nitrogen adsorption-desorption measurement on a Belsorp-Max (MicrotracBEL) conducted at -196 °C, in which the samples were treated at 350 °C for 3 h prior to the measurement. The calculation of BET and t-plot on the hierarchical samples follow as reported by Rouquerol [9] et.al. and Bosnar [10] et.al., respectively. The elemental analyses were carried out on an Inductively Coupled Plasma-Atomic Emission Spectrometer (ICP-AES, Shimadzu ICPE-9000). Meanwhile, temperature-programmed ammonia desorption (NH_3-TPD) profiles were recorded on a BELCAT-A (MicrotracBEL). ^{27}Al MAS NMR spectra were obtained on a JEOL ECA-600 spectrometer using a 4 mm ZrO_2 rotor with the spinning rate at 15kHz. The UV-Vis DRS spectrum was obtained from a V-650 spectrophotometer (JASCO), in which prior to the measurement, the sample was dehydrated in air at 550 °C for 4 h. The quantities of Brønsted and Lewis acid sites were evaluated by pyridine and collidine adsorption experiment using FTIR (JASCO FT/IR-4100) equipped with a mercury cadmium telluride (MCT) detector. First, the sample was pressed in a self-supporting disk (20 mm diameter) and then placed in an IR cell attached to a conventional closed-gas circulation system [11],[12]. Then, the pretreatment was carried out by the IR cell heated to 450 °C under vacuum, conducted for 1 h, and then

cooled to 150 ^{0}C for pyridine and the room temperature for collidine prior to the adsorption experiment. Subsequently, the spectrum was recorded and used as a background. After that, the probe molecule was introduced into the cell and then vacuumed until the vacuum condition for desorbing the physically adsorbed pyridine/collidine. Then, the temperature of the IR cell was increased to 250 °C for pyridine and 100 °C for collidine, kept for 15 mins, then cooled to 150 °C or room temperature and followed by a recording of the spectrum. The concentration of Brønsted and Lewis acid sites were calculated by Lambert-Beer's law [8], and the extinction coefficients were used: Brønsted (1.13 cm/μmol) and Lewis (1.28 cm/μmol) [13] for pyridine; Brønsted (8.1 cm/μmol) for collidine [14].

3.2.3. Catalytic reaction

The reaction conditions set up in this Chapter were the same as in Chapter 2. The catalytic reactions were conducted by using a fixed-bed flow reactor connected to an online Gas Chromatograph with an FID detector. The zeolites were shaped to be pellet form with a size of 500-1000 μm without a binder, and they were loaded into a quartz tubular flow microreactor (6 mm inner diameter) with a weight of 35 mg.

The conversion of methanol and the product selectivity were calculated on the basis of carbon number by following these formulas:

Conversion (%) = {1-(C-atoms of reactant $_{output}$)/C-atoms of reactant $_{input}$)} x 100

Product selectivity (%) = {C-atoms of the product/(C-atoms of reactant $_{input}$ – C-atoms of reactant $_{output}$)} x 100.

The methanol-to-olefins (MTO) reaction was performed at 450 ^{0}C with a partial pressure of 15 kPa and a W/F of 11.54 g-cat h mol^{-1} for methanol. Before the reaction, the catalyst was activated at 550 ^{0}C for 1 h in flowing Ar gas. The reaction products were analyzed by an online GC-FID with an HP-PLOT/Q capillary as the column.

3.3. Results and discussion

3.3.1. Varying crystallization temperature

3.3.1.1. Synthesis

Figure 3.1 exhibited the MFI framework was possessed by either the microporous ZSM-5 or the hierarchical ZSM-5, which was indicated by the emergence of the typical peaks of MFI framework at 7-9^0 2θ (the doublet peaks) and 22-25^0 2θ (the triplet peaks) [16]. The crystallinity possessed by all hierarchical ZSM-5 was relatively similar to the microporous ZSM-5, except Mic_Z5_[TPA[_200. The lower crystallinity on Mic_Z5_[TPA]_200 could be due to the small-sized crystals, in which the appearance of the broadened XRD peaks ascribed to the formation of small-sized crystals [17]. Based on the small angle patterns of XRD, all the hierarchical samples demonstrated the emergence of a single peak at around 2θ = 1.8^0. The small angle patterns of XRD from MCM-41 commonly exhibited three peaks at 2.5^0, 4.25^0, and 4.81^0, which was associated with the 100, 110, and 200 reflections of regular two-dimensional hexagonal structure [18]. Hence, it could be concluded that the hierarchical ZSM-5 zeolites had an irregular mesoporous structure. Even, it became worse when the crystallization temperature was increased to either Hi_Z5_[TPA+Na] or Hi_Z5_[TPA].

The addition of a surfactant as mesoporogen was impacted on the crystal size, as shown in **Figure 3.2**. Both Mic_Z5_[TPA+Na] and Mic_Z5_[TPA] had small-sized crystals with a typical crystal morphology of MFI (a coffin-like crystal), except Mic_Z5_[TPA]_200 (**Figure 3.2.(F)**). **Figure 3.2.(F)** showed the bigger crystals were composed of the aggregation of ultra-small-sized crystals, which corresponds to the result in **Figure 3.1**. Whereas, the hierarchical ZSM-5 (Hi_Z5_[TPA+Na] and Hi_Z5_[TPA]) either synthesized at 180 ^{0}C or at 200 ^{0}C possessed big-sized crystals with the same morphology as the microporous ZSM-5. However, the well-homogeneity of the hierarchical structure was not achieved, which was shown by the presence of a rough surface on the crystal surface. It indicated the higher temperature did not

influence the crystal size and morphology and the degree of homogeneity of the hierarchical structure.

3.3.1.2. Physicochemical properties

Figure 3.3. demonstrated the emersion of a hysteresis loop and a mesoporous step on both Hi_Z5_[TPA+Na] and Hi_Z5_[TPA] samples. A mesoporous step is a sharp increase in adsorption volume observed at a relative pressure of ≈0.3-0.5 and a hysteresis loop occurs due to capillary condensation, which are correlated to mesopore filling [19],[10],[20],[21],[22]. Therefore, it could be concluded that all hierarchical ZSM-5 zeolites contained a mesoporous structure. However, when the crystallization temperature enhanced to 200 ^{0}C, the mesoporous step became flatter either on Hi_Z5_[TPA+Na] or Hi_Z5_[TPA], which indicated the amount of the existing mesopore was reduced, and the structure formation was more led to the microporous structure. Meanwhile, the microporous samples showed a type I isotherm, which is the typical isotherm of the micropore materials [16].

Textural properties of the samples are listed in **Table 3.1**. S_{BET} influenced enhancement on the microporous ZSM-5 when the crystallization temperature was increased, but the opposite trend occurred on the hierarchical ZSM-5. This trend also occurred in S_{meso} and the pore size distribution. It denoted that a higher crystallization temperature would lead to the formation of mesopore (intercrystalline) for the microporous ZSM-5 zeolites and, vice versa, the formation of micropore for the hierarchical ZSM-5 zeolites. On the contrary, the impact of the higher crystallization temperature resulted in a reduction and an increase of S_{mic} on the microporous ZSM-5 and the hierarchical ZSM-5, respectively. However, it enhanced V_{mic} either on the microporous ZSM-5 or the hierarchical ZSM-5. Meanwhile, the deviation of Hierarchy Factor (HF), an index for the contribution of micropore volume to the total pore volume and the contribution of mesopore surface area to the total surface area of the sample are weight [23], between Hi_Z5_[TPA+Na] and Hi_Z5_[TPA] was not too significant. At low

crystallization temperature, Hi_Z5_[TPA+Na]_180_4.4 had a higher value of HF (0.06) than Hi_Z5_[TPA]_180_4.4 (0.05), while at high temperature, it was in reverse (Hi_Z5_[TPA+Na]_200_4.4 of 0.06 and Hi_Z5_[TPA]_200_4.4 of 0.07). A higher HF indicates the formation of more mesopores with preserved micropores [24].

Regarding the chemical properties (**Table 3.2**), the hierarchical ZSM-5 exhibited a lower number of strong acid amounts compared to the microporous ZSM-5. Furthermore, the increased crystallization temperature resulted in a decline in the number of strong acid amounts on both the hierarchical ZSM-5 and the microporous ZSM-5 zeolites. This trend also occurred in the strength of acid in those zeolites, as shown in **Figure 3.4**. It indicated that overheating in a crystallization process caused the strength of acid in zeolite to become weaker.

The strength of acid sites based on the FTIR-Pyridine measurement disclosed that the hierarchical ZSM-5 without Na had a higher amount of Brønsted acid sites than the hierarchical ZSM-5 with Na. The amount of its acid sites was not influenced by the increase in crystallization temperature, but its increase affected the amount of Lewis acid sites. It denoted that the higher crystallization temperature yielded a big impact on acid sites located on the mesopores and or the defect sites due to the Lewis acid sites being dominantly located in those locations [10]. Meanwhile, the microporous ZSM-5 possessing the amount of Brønsted acid sites was relatively the same, except Mic_Z5_[TPA]_200. The lower amount could be due to the crystal size being too small, as the ultra-small-sized crystals enhanced the formation of Lewis acid sites [8].

On the other hand, an analysis of the Brønsted acid sites located in the mesopores and/or the external surface (which were calculated based on the collidine adsorption) was carried out. The interpretation of collidine adsorption spectra was conducted by deconvolution of the spectra, in which the wavenumber of 1619 and 1633 cm^{-1} were assigned to collidine adsorbed

on silanol and Lewis sites, respectively. The wavenumbers 1638 cm^{-1} and 1650 cm^{-1} were assigned to collidine adsorbed on Brønsted sites [14],[25]. Based on its calculation, the hierarchical ZSM-5 exhibited a higher number of the Brønsted acid sites than the microporous samples. It implied the occurrence of the aluminum migration process from the micropores to the mesopores and/or the external surface. However, the amount difference of its acid sites was not significant between Hi_Z5_[TPA+Na] and Hi_Z5_[TPA].

3.3.1.3. Al distribution

As shown in **Figure 3.5**, both the microporous ZSM-5 and the hierarchical ZSM-5 zeolites demonstrated the appearance of peaks at ca. 55 ppm and 0 ppm. These peaks are associated with tetrahedrally coordinated Al in the framework (55 ppm) and octahedrally coordinated Al in the extra-framework (0 ppm) [26],[27]. Meanwhile, Al distribution of the microporous and the hierarchical ZSM-5 zeolites was exhibited in **Table 3.3**. The microporous samples demonstrated the same result as our previous report [26],[27], in which the ZSM-5 with Na possessed Al more located in the channels (56 ppm) than in the channel intersections (54 ppm), which revealed in the higher value of T_{56}/T_{54} for Mic_Z5_[TPA+Na]. However, the hierarchical ZSM-5 represented the reversed trend, in which Hi_Z5_[TPA+Na] had a lower value of T_{56}/T_{54} than Hi_Z5_[TPA]. This indicated some Al, which should be located in the channels of micropores, was migrated to the mesopores and/or the external surface. Furthermore, it was revealed that crystallization temperature influenced Al distribution on Hi_Z5_[TPA] only, in which the higher temperature resulted in a ratio of T_{56}/T_{54} decreased. This implied that the role of sodium in controlling Al distribution in the framework reached the maximum performance at the crystallization temperature of 180 ^{0}C.

Table 3.4 demonstrated the change of Al pairs distribution in the framework after the modification of the structure. Calculation of Al pairs distribution determined by the deconvolution of Co(II) UV-Vis DRS spectra from Co-ZSM-5 samples, which referred to

works of dědeček [28] et.al., and Liang [29] et.al., in which α-type Co(II) ions were found in the straight channel (band at 15,100 cm^{-1}), β-type Co(II) ions were located in the channel intersection (band at 16,000, 17,150, 18,600, and 21,200 cm^{-1}) and γ-type Co(II) ions were present in the sinusoidal channel (band at 20,100 and 22,000 cm^{-1}). The hierarchical ZSM-5 showed enhancement of Al pairs distribution in the channel intersections compared to the microporous ZSM-5. This denoted that at high crystallization temperatures, the surfactant (CTAB) forced the formation of Al pairs. It could be due to the micelle form of the surfactant not being preserved at high temperatures [30], so the individual surfactants were most likely to enter the micropores with the cationic heads of surfactant leading to the channel intersections. Moreover, the hierarchical ZSM-5 with Na exhibited a higher Al pairs distribution than the hierarchical ZSM-5 without Na which was an opposite trend with the microporous ZSM-5, indicating sodium influenced the formation of Al pairs as well.

3.3.1.4. Catalytic reaction

Figure 3.6 demonstrated that either the microporous ZSM-5 or the hierarchical ZSM-5 produced high selectivity on ≥C5s compounds, but the microporous ZSM-5 was superior. However, the hierarchical ZSM-5 was more selective to produce a lower olefins, especially propene, than the microporous ZSM-5. This indicated that the hierarchical structure gave rise to a better performance in lower olefins production compared to the micropore structure only. Furthermore, the impact of Al distribution on methanol conversion was observed, in which the samples having Al more located in the channel intersections produced more ethene. Based on the dual-cycle concept proposed by Olsbye and co-worker [30] that ethene was formed from the aromatic-based cycle involving the aromatization of higher alkenes formed in the alkene methylation or cracking cycle. The aromatic-based cycle was preferably carried out at the wider space, i.e., the channel intersections. Thus, this typical product could be used to identify the aluminum location.

In the methanol-to-olefins reaction, hydrocarbon pool mechanisms, which suggest the presence of hydrocarbon species working as an intermediate promotor inside the micropore of the zeolite, have been widely accepted based on experimental and theoretical evidence [31],[32]. **Figure 3.7** exhibited the ratio of propene-to-ethene selectivities (C3=/C2=) from all samples. This ratio could serve as an indicator to identify the hydrocarbon pool species of the MTO reaction due to short- and long-chain olefins are preferentially produced through aromatic and olefinic hydrocarbon pool species, respectively [1]. The Mic_Z5_[TPA+Na] (the microporous ZSM-5 with Na) and Hi_Z5_[TPA] (the hierarchical ZSM-5 without Na) showed a higher ratio compared to Mic_Z5_[TPA] and Hi_Z5_[TPA+Na], respectively. It indicated the distribution of Al was more concentrated in the channels than the channel intersections.

3.3.2. Varying the mesoporogen concentration

Figure 3.8 demonstrated the hierarchical ZSM-5 with a lower concentration of mesoporogen (Hi_Z5_[TPA+Na]_180_2.2 and Hi_Z5_[TPA]_180_2.2) had a MFI framework, but the intensity was slightly lower than the hierarchical ZSM-5 with a higher concentration (Hi_Z5_[TPA+Na]_180_4.4 and Hi_Z5_[TPA]_180_4.4). Furthermore, the regularity of the produced mesoporous structure was reduced. It indicated that higher mesoporogen concentration would lead to the formation of a more well-ordered mesoporous structure.

A lower concentration of mesoporogen did not influence the crystal morphology, in which the observed morphology was coffin-like either on a higher concentration or a lower concentration, as shown in **Figure 3.9**. However, it influenced the resulting textural properties and the isotherm profile of nitrogen adsorption-desorption, as exhibited in **Table 3.5** and **Figure 3.10**, respectively. Both on Hi_Z5_[TPA+Na]_180_2.2 and Hi_Z5_[TPA]_180_2.2 samples demonstrated the produced “mesoporous step” was flatter compared to Hi_Z5_[TPA+Na]_180_4.4 and Hi_Z5_[TPA]_180_4.4, respectively (**Figure 3.10**). It implied that the amount of mesopore formed on those samples was lower, and it was caused by the low

quantity of mesoporogen was added into the synthetic gel. This result was reflected in S_{meso} and V_{meso} that possessed by Hi_Z5_[TPA+Na]_180_2.2 and Hi_Z5_[TPA]_180_2.2 (**Table 3.5**), in which they revealed the lower values compared to the hierarchical ZSM-5 with a higher concentration (Hi_Z5_[TPA+Na]_180_4.4 and Hi_Z5_[TPA]_180_4.4). Furthermore, the impact of the low concentration of mesoporogen resulted in the pore size and S_{BET} being smaller and lower, respectively, denoting that the formed structure was directed to the formation of the microporous structure, which was supported by a higher value of S_{mic} and V_{mic}. However, Hi_Z5_[TPA+Na]_180_2.2 and Hi_Z5_[TPA]_180_2.2 exhibited a higher Hierarchy Factor (HF) with the same value of 0.08 compared to Hi_Z5_[TPA+Na]_180_4.4 (value of 0.06) and Hi_Z5_[TPA]_180_4.4 (value of 0.05), indicating more created mesopores with preserved micropores [24].

Table 3.6 revealed the hierarchical ZSM-5 zeolites with a lower concentration of mesoporogen possessing a number of strong acid amounts were higher compared to the hierarchical ZSM-5 with a higher concentration. Moreover, based on the FTIR-Pyridine measurement, they had a strength of acid sites being stronger, which was shown by the higher amount of Brønsted acid sites. It indicated that the microporous structure was more dominant on the hierarchical ZSM-5 with a lower concentration of mesoporogen as the Brønsted acid sites were associated mostly with the microporous structure [10]. Furthermore, analysis of collidine adsorption to estimate the amount of Brønsted acid sites located in the mesopore and/or the external surface showed either Hi_Z5_[TPA+Na]_180_2.2 or Hi_Z5_[TPA]_180_2.2 had a higher amount of Brønsted acid sites than Hi_Z5_[TPA+Na]_180_4.4 and Hi_Z5_[TPA]_180_4.4, respectively, with the highest amount was possessed by Hi_Z5_[TPA+Na]_180_2.2. It implied that the lower concentration of mesoporogen would result in more Al migration to the mesopore and/or the external surface. This could be due to the uncompleted-micelle formation (a low degree of regularity of the

mesoporous structure (**Figure 3.8**)), resulting in the competition between TPA^+ and CTA^+ for attracting aluminosilicate species and subunits that contain aluminum being uncontrolled so that Al attraction by CTA^+ could occur anytime and anywhere.

As shown in **Figure 3.11**, either Hi_Z5_[TPA+Na]_180_2.2 or Hi_Z5_[TPA]_180_2.2 showed the appearance of the peaks at ca. 55 ppm and 0 ppm, which were associated with the tetrahedrally coordinated Al in the framework (55 ppm) and octahedrally coordinated Al in the extra-framework (0 ppm) [26],[27]. While, Al distribution on the hierarchical ZSM-5 that varied mesoporogen concentration was demonstrated in **Table 3.7**. All the hierarchical ZSM-5 with a lower concentration exhibited a lower value of T_{56}/T_{54} ratio than the samples with a higher concentration, with Hi_Z5_[TPA+Na]_180_2.2 having the lowest value. It denoted the Al migration process was much occurred in the samples with a lower concentration, which supported the result in **Table 3.6**.

Besides influencing the Al migration process, a lower concentration of mesoporogen also affected the Al pairs distribution in the framework, as exhibited in **Table 3.8**. Both Hi_Z5_[TPA+Na]_180_2.2 and Hi_Z5_[TPA]_180_2.2 samples possessed a higher and lower Al pairs distribution in the channel intersections and in the channels, respectively, than the hierarchical ZSM-5 with a higher concentration (Hi_Z5_[TPA+Na]_180_4.4 and Hi_Z5_[TPA]_180_4.4), with the highest value on Hi_Z5_[TPA+Na]_180_2.2. This was probably due to many individual surfactants not creating the perfect micelle form, resulting in those individuals probably entering the micropores with the cationic head of surfactant leading to the channel intersections following the location of Al and the hydrophobic tails in the channels. Consequently, it was impacted toward Al pairs distribution in the channels becoming lower, as the polarity in the channels was changed to be more hydrophobic.

Figure 3.12 showed that the hierarchical ZSM-5 with a lower concentration of

mesoporogen gave rise to a similar conversion of methanol (~100%) with the hierarchical ZSM-5 having a higher concentration. All samples produced the highest selectivity on bulky compounds (≥C5s), followed by propene, with the highest selectivity of propene occurring on [TPA] samples. The ratio of C3=/C2= selectivity on [TPA] samples demonstrated a higher value compared to [TPA+Na] samples. It indicated Al distribution was more concentrated in the channels than in the channel intersections, which supported the result in **Table 3.7**.

Because the hierarchical ZSM-5 with a lower mesoporogen concentration showed a very high Al pairs distribution in the channel intersections in **Table 3.8**, which indicated this typical ZSM-5 was easily deactivated due to a higher percentage of Al pairs in the channel intersections would increase the coke formation [26], the durability test of its catalyst was carried out as shown in **Figure 3.13**. It was clearly observed that the durability of Hi_Z5_[TPA]_180_2.2 in methanol conversion was shorter than the control sample (Mic_Z5_[TPA]_180). This was caused by a higher coke deposition in Hi_Z5_[TPA]_180_2.2 (8.07%) than Mic_Z5_[TPA]_180 (2.8%), as demonstrated in **Figure 3.14**.

3.3.3. Influence of pH adjustment and timing mesoporogen addition

To investigate the influence of pH on the formation of the hierarchical structure and Al distribution, acetic acid was used to control the pH of the mixture, and the list of pH solutions is shown in **Table 3.9**.

Figure 3.15 revealed either the hierarchical ZSM-5 without the pH adjustment (Hi_Z5_[TPA+Na]_180_4.4_WApH; Hi_Z5_[TPA]_180_4.4_WApH) or the hierarchical ZSM-5 were switched timing mesoporogen addition with microporogen (Hi_Z5_[TPA+Na]_180_4.4_Csw; Hi_Z5_[TPA]_180_4.4_Csw) had MFI framework (emerging the doublet peaks at 7-9^0 2Θ and the triplet peaks at 22-25^0 2Θ [16]). However, those types of hierarchical ZSM-5 zeolites did not show the regularity of the mesoporous

structure at all, as demonstrated by the control samples (Hi_Z5_[TPA+Na]_180_4.4 and Hi_Z5_[TPA]_180_4.4). It indicated that the pH of the synthetic gel and the order of microporogen and mesoporogen addition into the synthetic gel were crucial to forming the ordered mesoporous structure. Furthermore, the influence of those varied treatments resulted in a change in the crystal size (**Figure 3.16**). Both the samples with timing mesoporogen addition switched (Hi_Z5_[TPA+Na]_180_4.4_Csw and Hi_Z5_[TPA]_180_4.4_Csw) and the samples with the pH without adjustment (Hi_Z5_[TPA+Na]_180_4.4_WApH and Hi_Z5_[TPA]_180_4.4_WApH) exhibited the smaller crystal size that the control samples. Moreover, those crystal surfaces experienced a change, in which [TPA+Na]_180_4.4_Csw and [TPA]_180_4.4_Csw possessed a half-smooth and a half-rough crystal surface, whereas the [TPA+Na]_180_4.4_WApH and [TPA]_1804.4_WApH possessed a perfectly smooth crystal surface.

The isotherm of nitrogen adsorption-desorption (**Figure 3.17**) exhibited that the hierarchical ZSM-5 with timing mesoporogen addition switched had a small mesoporous step, while the hierarchical ZSM-5 without pH adjustment did not show a mesoporous step at all. This denoted that the samples with timing mesoporogen addition switched had a very small amount of mesopore inside the framework. Whereas, the samples without pH adjustment were most likely not possessing the mesoporous structure inside the framework. Furthermore, the textural properties (**Table 3.10**) revealed that S_{mic}, and V_{mic} possessed by those samples were relatively high compared to the control samples. Even, their S_{meso} was very low. It implied that the microporous structure almost fully constructed those samples. This indication was strengthened by the pore size of those samples, which was in the micropore area (< 2nm). However, the Hierarchy Factor (HF) produced by them demonstrated a relatively high value, i.e., 0.12 for Hi_Z5_[TPA+Na]_180_4.4_Csw and Hi_Z5_[TPA+Na]_180_4.4_WApH and 0.13 for Hi_Z5_[TPA]_180_4.4_Csw and Hi_Z5_[TPA]_180_4.4_WApH. Its high value did

not show directly the high degree of hierarchical structure (a high HF shows more mesopore formed with preserved micropore), but it indicated the samples were mostly microporous structures as HF ≤ 0.1 also indicates zeolites which were mostly microporous or mesoporous nature [23].

As explained in the experiment section, the pH of the mixture was adjusted by the addition of acetic acid. pH (alkalinity) in the synthesis mixture plays a significant role in the nucleation and crystal growth [17]. An increase in pH will accelerate crystal growth and shorten the induction time [35]. Therefore, a reduction of pH will increase the induction time and condensation, resulting in increasing interaction of aluminosicate species and/or the subunits with microporogen and mesoporogen before growing to be crystal. On the other hand, acetic acid has another role in creating a hierarchical structure, in which it reduces the repulsive forces of the surfactant heads, leading thus to an increase in the micelle packing parameter and hence the denser micelle arrangement [36],[37] so that the affinity between the micelles and the aluminosilicate species enhanced. Moreover, acetic acid can reduce the polymerization rate of subunits due to the negative charge of CH_3COO^- will give the repulsive forces to the subunits.

Table 3.11 disclosed that either the hierarchical ZSM-5 with timing mesoporogen addition switched or the hierarchical ZSM-5 without pH adjustment had a higher number of strong acid amounts compared to the control samples. Furthermore, the strength of acid sites possessed by them was stronger, as shown by the high number of Brønsted acid sites. Moreover, they had a higher ratio of Brønsted to Lewis (B/L) acid sites. Those denoted that they had a more microporous structure than the mesoporous structure compared to the control samples. On the other hand, analysis of the number of Brønsted acid sites located in the mesopore and/or the external surface by FTIR characterization using collidine as a probe molecule showed the hierarchical ZSM-5 with timing mesoporogen addition switched (Hi_Z5_[TPA+Na]_180_4.4_Csw and Hi_Z5_[TPA]_180_4.4_Csw) produced lower values

with similar values among them compared to the control samples. On the other hand, the hierarchical ZSM-5 without pH adjustment disclosed lower values with different trends compared to the control samples. The trend demonstrated by the samples was similar to the original ZSM-5 (Mic_Z5_[TPA+Na]_180 and Mic_Z5_[TPA]_180) in **Table 3.2**. Therefore, it indicated these values were probably come from the external surface which supported by the perfect smooth crystal surface in **Figure 3.16**.

Either the hierarchical ZSM-5 with timing mesoporogen addition switched or the hierarchical ZSM-5 without pH adjustment emerged the peak at ca. 55 ppm and at 0 ppm, which corresponded to the tetrahedrally coordinated Al in the framework and octahedrally coordinated Al in the extra-framework, respectively [26],[27]. Meanwhile, Al distribution over the hierarchical ZSM-5 that the pH without adjustment and timing mesoporogen addition switched was demonstrated in **Table 3.12**. For the hierarchical ZSM-5 that timing mesoporogen addition switched, the ratio of T_{56}/T_{54} on Hi_Z5_[TPA+Na]_180_4.4_Csw was slightly higher than Hi_Z5_[TPA]_180_4.4_Csw, in which it was a reversed trend compared to the control samples. This trend was similar to the original ZSM-5 (Mic_Z5_[TPA+Na]_180 and Mic_Z5_[TPA]_180) in **Table 3.3**. It indicated that by this like-treatment approach, the Al distribution in the framework was not changed due to the arrangement of Al in the framework just started when microporogen (TPAOH) was added, and the rate of silicate polymerization with the presence of Na was increased [33],[34], so that there was not enough time for mesoporogen (in micelle form) to attract the aluminosilicate species and/or the subunits containing Al. On the other hand, the hierarchical ZSM-5 without pH adjustment exhibited the same trend as the control samples. This was probably due to some mesoporogen in the form of the individual surfactants (due to not forming micelle form), which have interacted with the aluminosilicate species, being attracted by the positive charge of the TPA^+, resulting in Al being more concentrated around the channel intersections. This process was further accelerated

by the presence of Na in the mixture.

The assumption of the individual surfactants involved in Al distribution in the channel intersections was supported by the result in **Table 3.13**. The hierarchical ZSM-5 without pH adjustment possessed a higher Al pairs distribution compared to the control samples, either the sample containing sodium or the sample without containing sodium. Furthermore, this result also occurred on the hierarchical ZSM-5 with timing mesoporogen addition switched due to this approach producing an irregular mesoporous structure as the hierarchical ZSM-5 without pH adjustment (**Figure 3.15**).

Figure 3.19 showed the impact of those treatments on the reaction of methanol conversion. Either the hierarchical ZSM-5 with timing mesoporogen addition switched or the hierarchical ZSM-5 without pH adjustment demonstrated a similar percentage of methanol conversion with the highest product selectivity on the bulky molecules (≥ C5s). Even, its value was higher than the control sample. However, the propene selectivity from those samples was dramatically lower than the control samples. It was due to those having a more microporous structure than the control samples, in which the result trend was the same as the original ZSM-5 in **Figure 3.6**. Meanwhile, the ratio of C3=/C2= selectivity shown in **Figure 3.20** revealed that Hi_Z5_[TPA+Na]_180_4.4_Csw had a slightly higher ratio than Hi_Z5_[TPA]_180_4.4_Csw, indicating Al distribution in the channels was higher on the sample with Na. Whereas, Hi_Z5_[TPA+Na]_180_4.4_WApH possessed a lower ratio than Hi_Z5_[TPA]_180_4.4_WApH, denoting Al distribution more concentrated in the channel intersections for the sample with Na. The results in **Table 3.11** supported those results.

3.4. Conclusions

The effect of the synthesis condition and the composition of the starting materials on the aluminum distribution in the hierarchical ZSM-5 intracrystalline has been investigated. For

the parameter of the crystallization temperature, the high crystallization temperature influenced not only aluminum distribution in the framework but also the hierarchical structure. Overheating crystallization temperature resulted in the enhancement of Al pairs distribution in the channel intersections, with a higher concentration on Hi_Z5_[TPA+Na]. However, the high crystallization temperature did not influence the ratio of Al distribution on the channels to the channel intersections, but it impacted on Hi_Z5_[TPA]. Moreover, a high crystallization temperature gave rise to an inhomogeneous structure between the microporous structure and mesoporous structure. In addition, it would lead to the formation of the microporous structure. Whereas for the parameter of the synthetic gel pH, the hierarchical ZSM-5 without pH adjustment (pH of ~14) possessed Al distribution was more concentrated in the channel intersection for Hi_Z5_[TPA+Na]_180_4.4_WApH, like the hierarchical ZSM-5 with pH adjustment which proved by ratio of T_{56}/T_{54} in the framework and ratio of C3=/C2= selectivity in the reaction of methanol conversion. Furthermore, the high pH of synthetic gel resulted in an increase of Al pairs distribution in the channel intersections. Meanwhile, the hierarchical structure produced by this treatment was not achieved. Even, it tends to the formation of the microporous structure only. On the other hand, Al distribution produced by the hierarchical ZSM-5 with timing mesoporogen addition into the synthetic gel switched to microporogen demonstrated the reversed trend with the hierarchical ZSM-5 synthesized using the original procedure. Its trend was the same as the original ZSM-5, in which the sample containing sodium (Hi_Z5_[TPA+Na]_180_4.4_Csw) had a higher ratio of T_{56}/T_{54} than the sample without containing sodium (Hi_Z5_[TPA+Na]_180_4.4_Csw). This result was also proved by the ratio of C3=/C2= selectivity in the methanol conversion. Moreover, it resulted in a higher percentage of Al pairs distribution in the channel intersections compared to the control samples. Whereas the produced hierarchical structure, this treatment produced the mesopore inside the framework very little, which was shown by the appearance of a very low mesoporous step,

indicating the microporous structure was more dominant than the mesoporous structure.

For the parameter of the composition of the starting materials, Al distribution on the hierarchical ZSM-5 with a lower concentration of mesoporogen (Hi_Z5_[TPA+Na]_180_2.2 and Hi_Z5_[TPA]_180_2.2) demonstrated the same trend as the hierarchical ZSM-5 with a higher concentration, in which Al distribution on Hi_Z5_[TPA+Na]_180_2.2 was more located in the channel intersections than Hi_Z5_[TPA]_180_2.2. This result was supported by the ratio of C3=/C2= selectivity in the methanol conversion reaction. Furthermore, the produced Al pairs distribution in the channel intersections was higher than the hierarchical ZSM-5 with a higher concentration, indicating the low concentration of mesoporogen would force the formation of Al pairs.

In short, this study gives valuable insight into the development of various zeolite catalysts (particularly in the hierarchical ZSM-5 zeolite) in terms of the correlation between the synthesis condition and the composition of the starting material toward aluminum distribution in the ZSM-5 zeolite to increase the selectivity of the catalytic process.

3.5. Figures and Tables

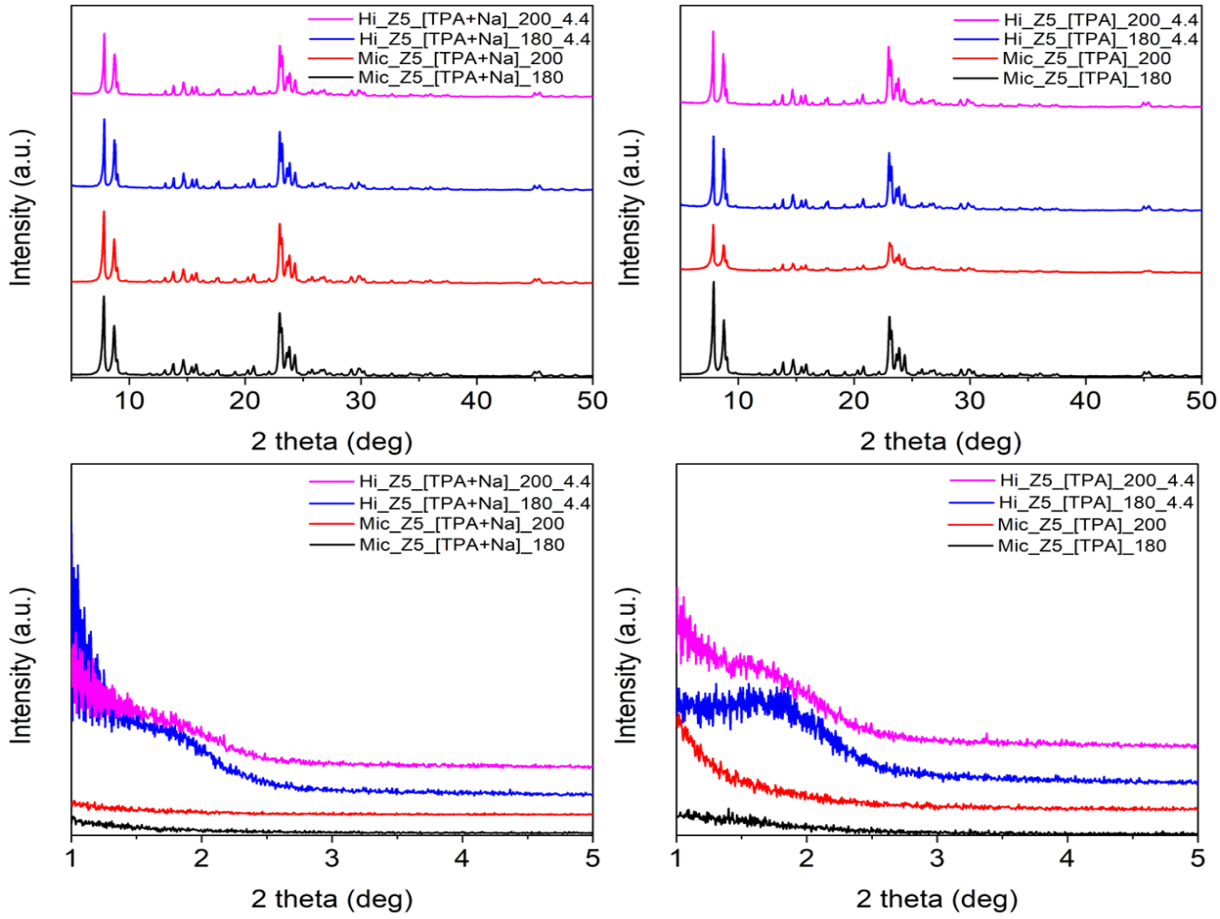

Figure 3.1. Wide and small angle patterns of XRD of the ZSM-5 with Na (left) and without Na (right).

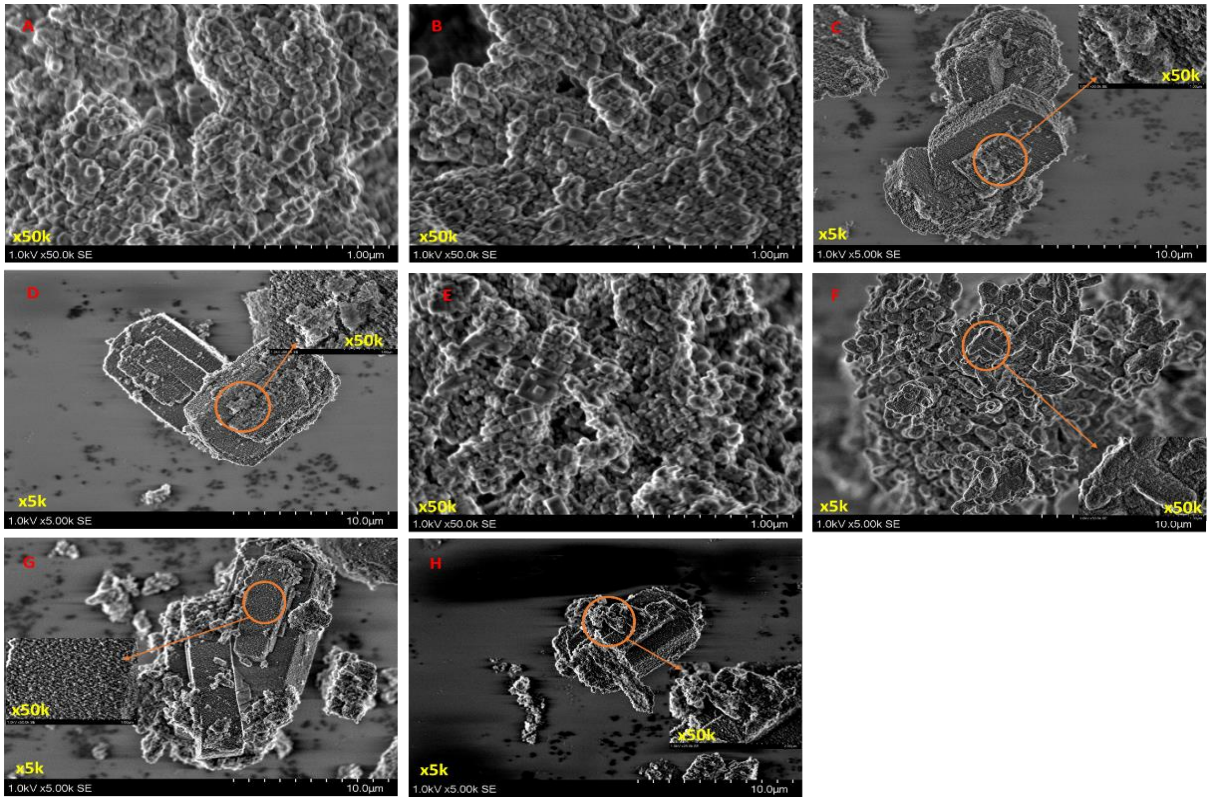

Figure 3.2. FE-SEM images from the microporous and hierarchical ZSM-5 zeolites: (A) Mic_Z5_[TPA+Na]_180; (B) Mic_Z5_[TPA+Na]_200; (C) Hi_Z5_[TPA+Na]_180_4.4; (D) Hi_Z5_[TPA+Na]_200_4.4; (E) Mic_Z5_[TPA]_180; (F) Mic_Z5_[TPA]_200; (G) Hi_Z5_[TPA]_180_4.4; (H) Hi_Z5_[TPA]_200_4.4

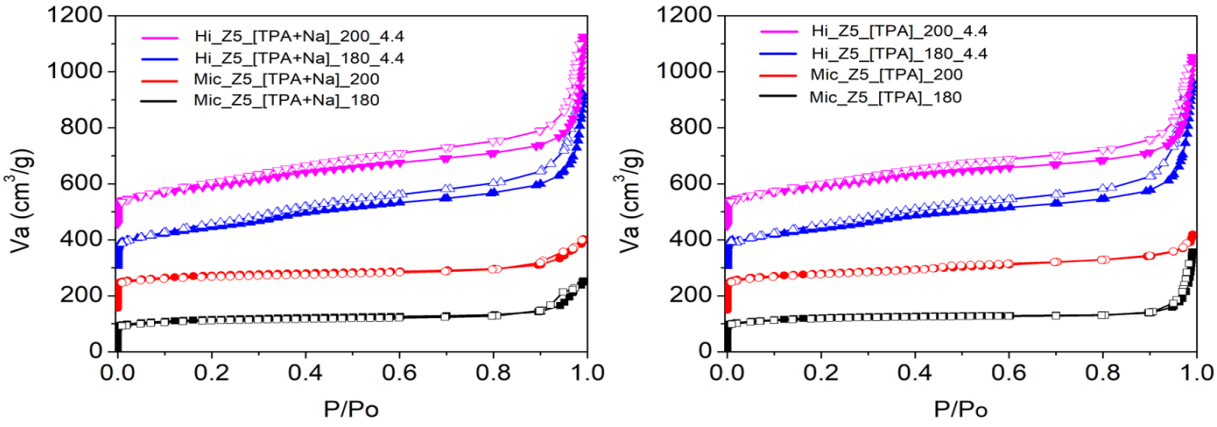

Figure 3.3. Adsorption-desorption isotherm of nitrogen on the ZSM-5 with Na (left) and without Na (right).

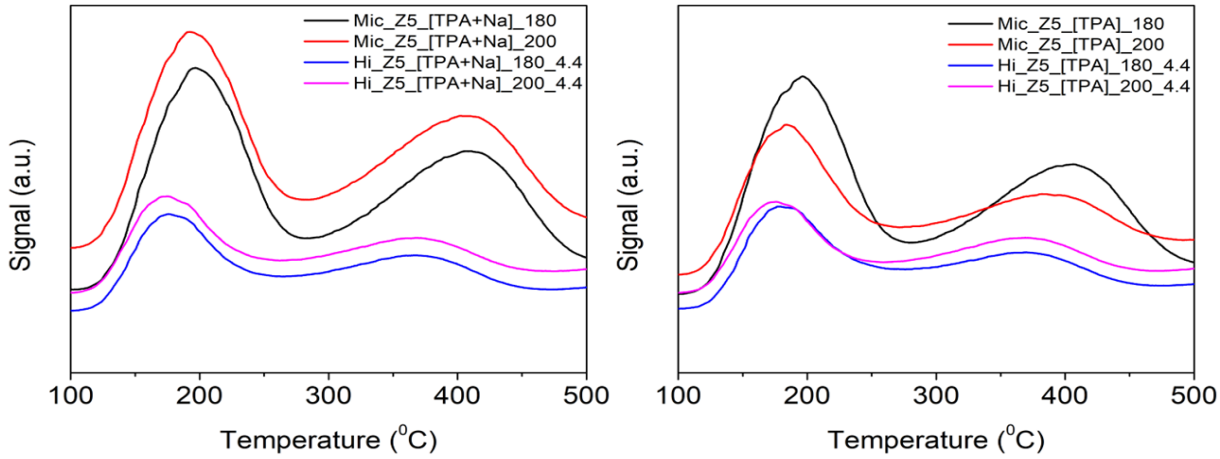

Figure 3.4. NH_3-TPD profile of microporous and hierarchical ZSM-5 with Na (left) and without Na (right).

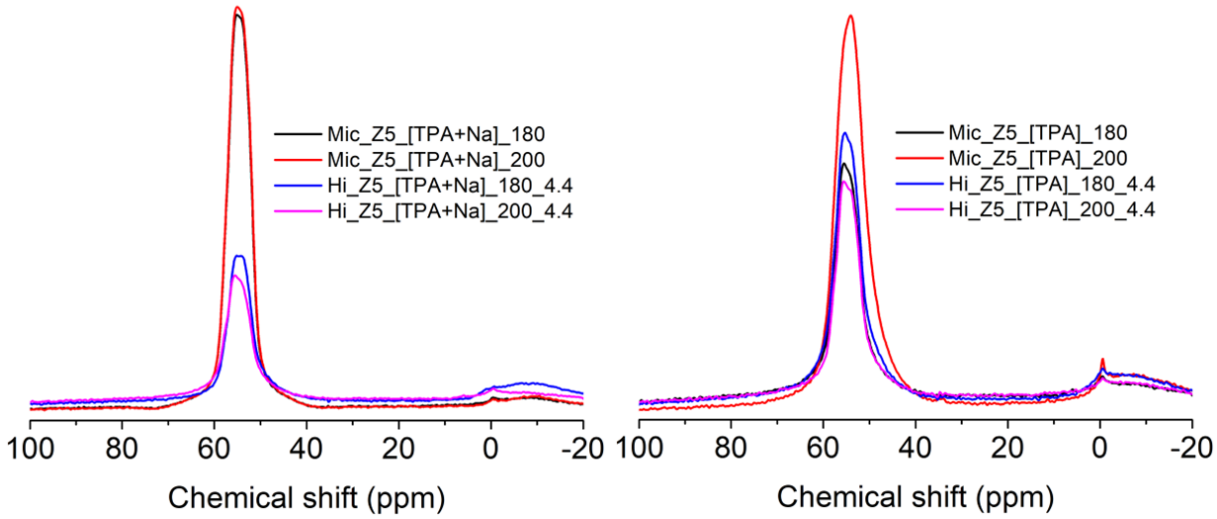

Figure 3.5. ^{27}Al MAS NMR spectra of the microporous and hierarchical ZSM-5 zeolites.

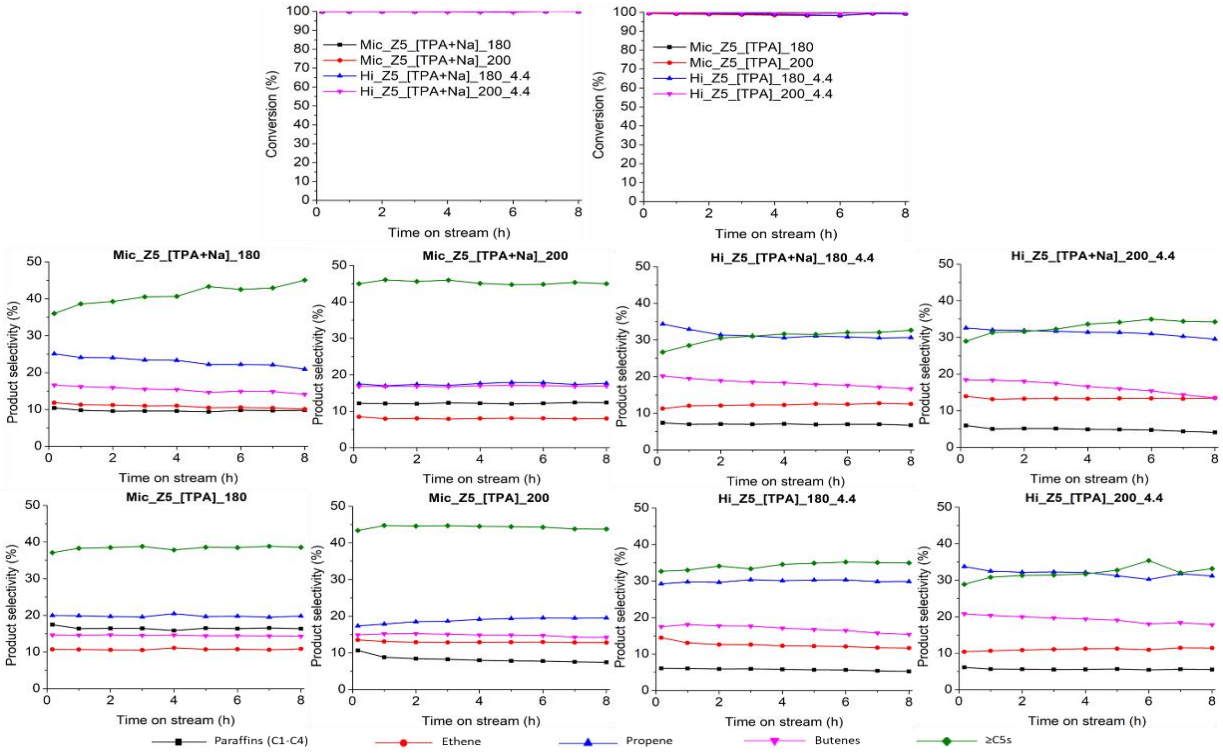

Figure 3.6. Product selectivity and conversion of methanol with time on stream (TOS) over the ZSM-5 with Na and the ZSM-5 without Na.

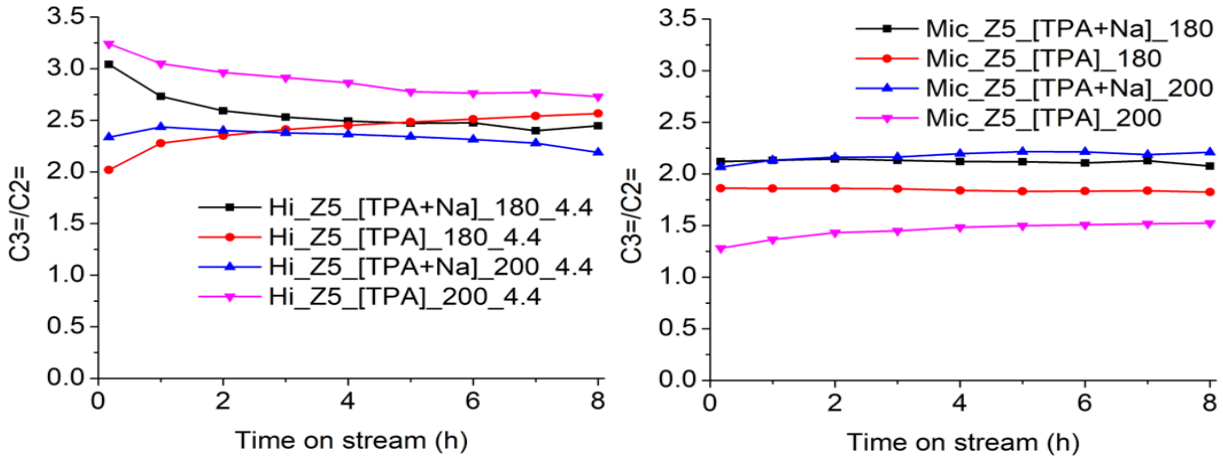

Figure 3.7. The ratio of C3=/C2= selectivities from the hierarchical and microporous ZSM-5.

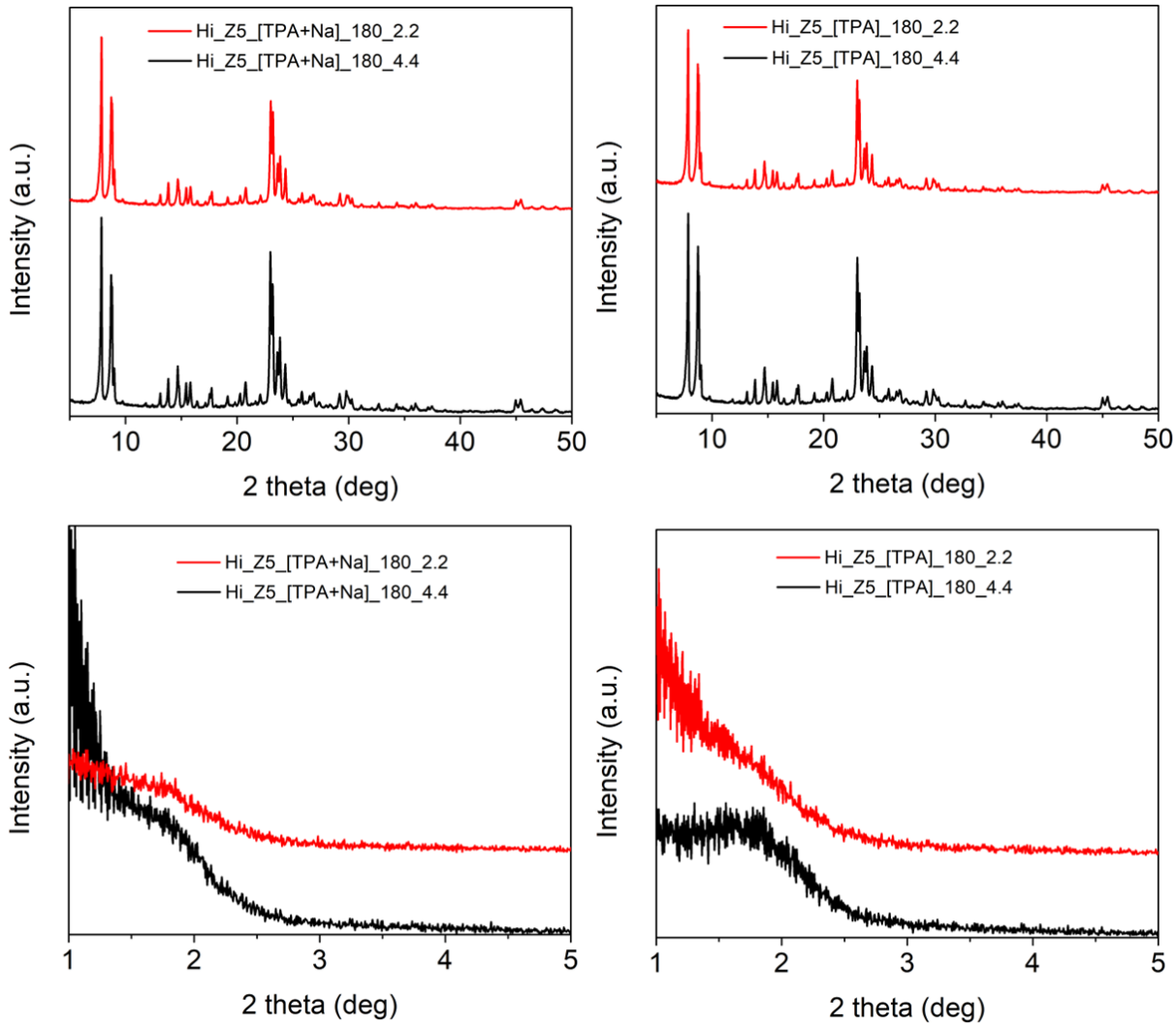

Figure 3.8. Wide and small angle patterns of XRD from the hierarchical ZSM-5 with varied mesoporogen concentration.

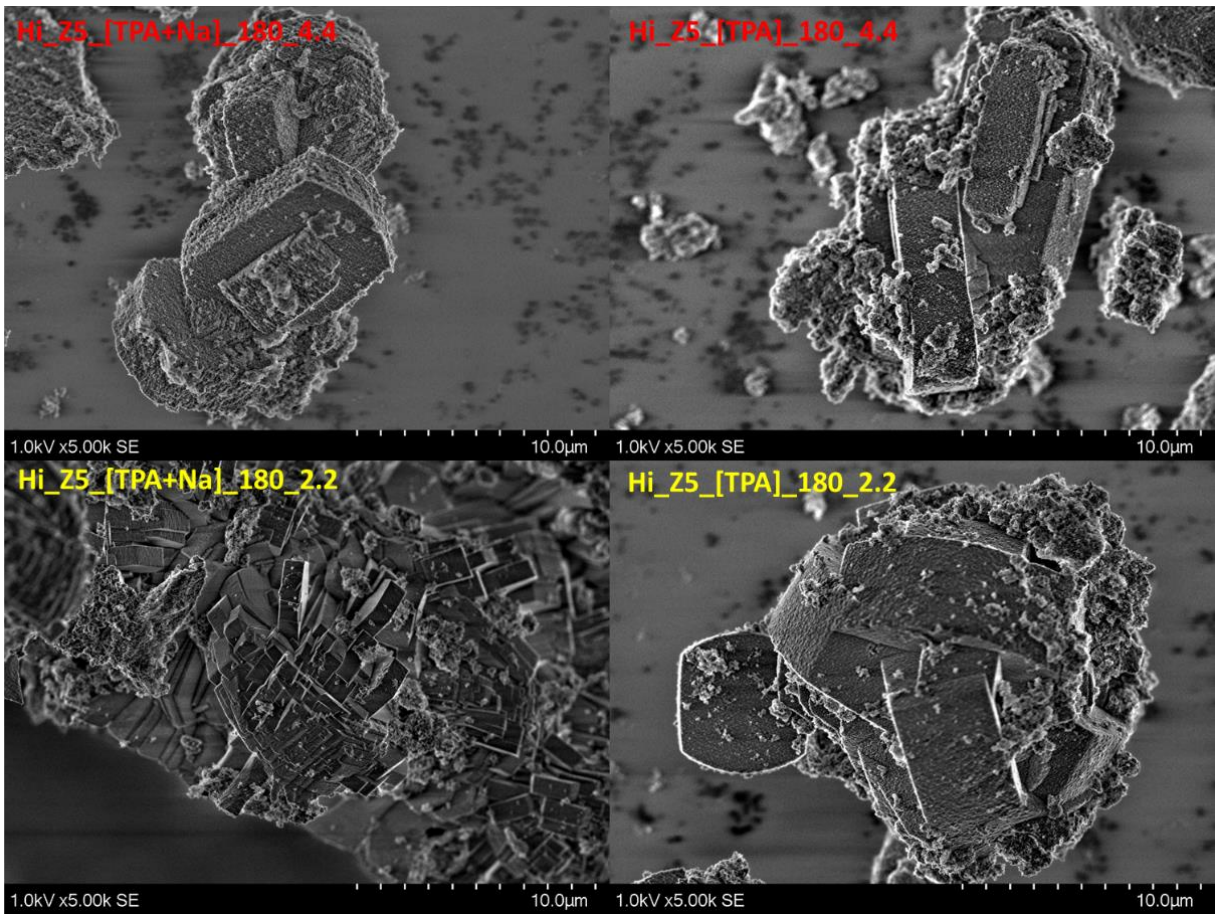

Figure 3.9. FE-SEM images from the hierarchical ZSM-5 with varied mesoporogen concentration.

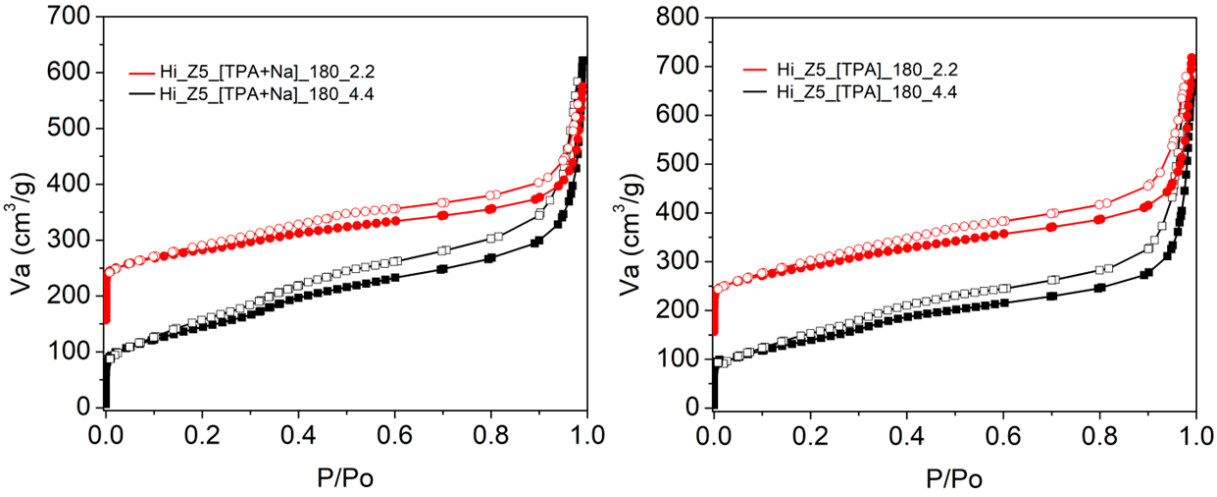

Figure 3.10. Adsorption-desorption isotherm of nitrogen from the hierarchical ZSM-5 with varied mesoporogen concentration.

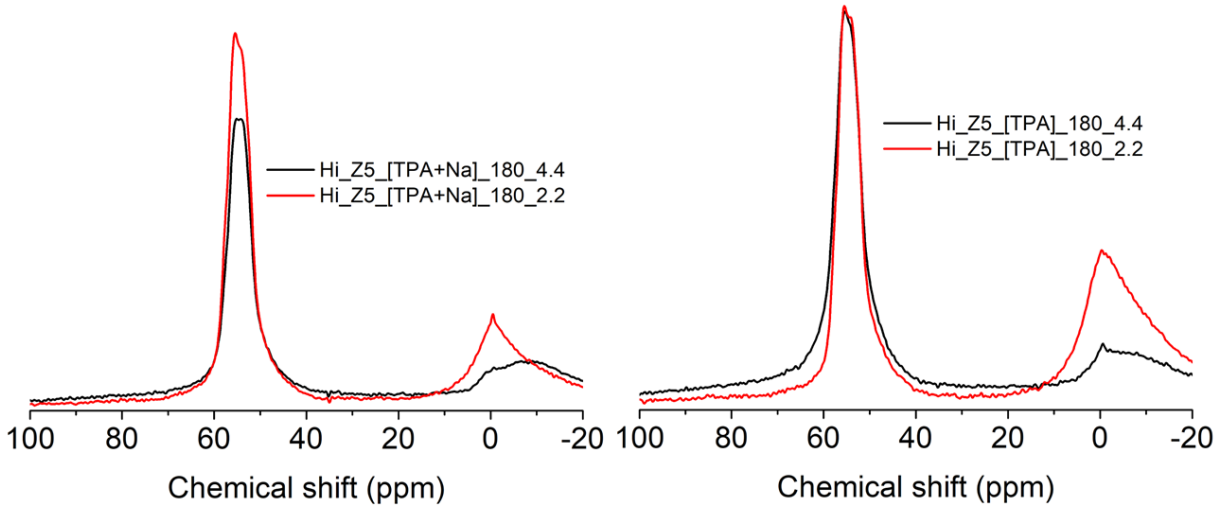

Figure 3.11. ^{27}Al MAS NMR spectra from the hierarchical ZSM-5 with varied mesoporogen concentration.

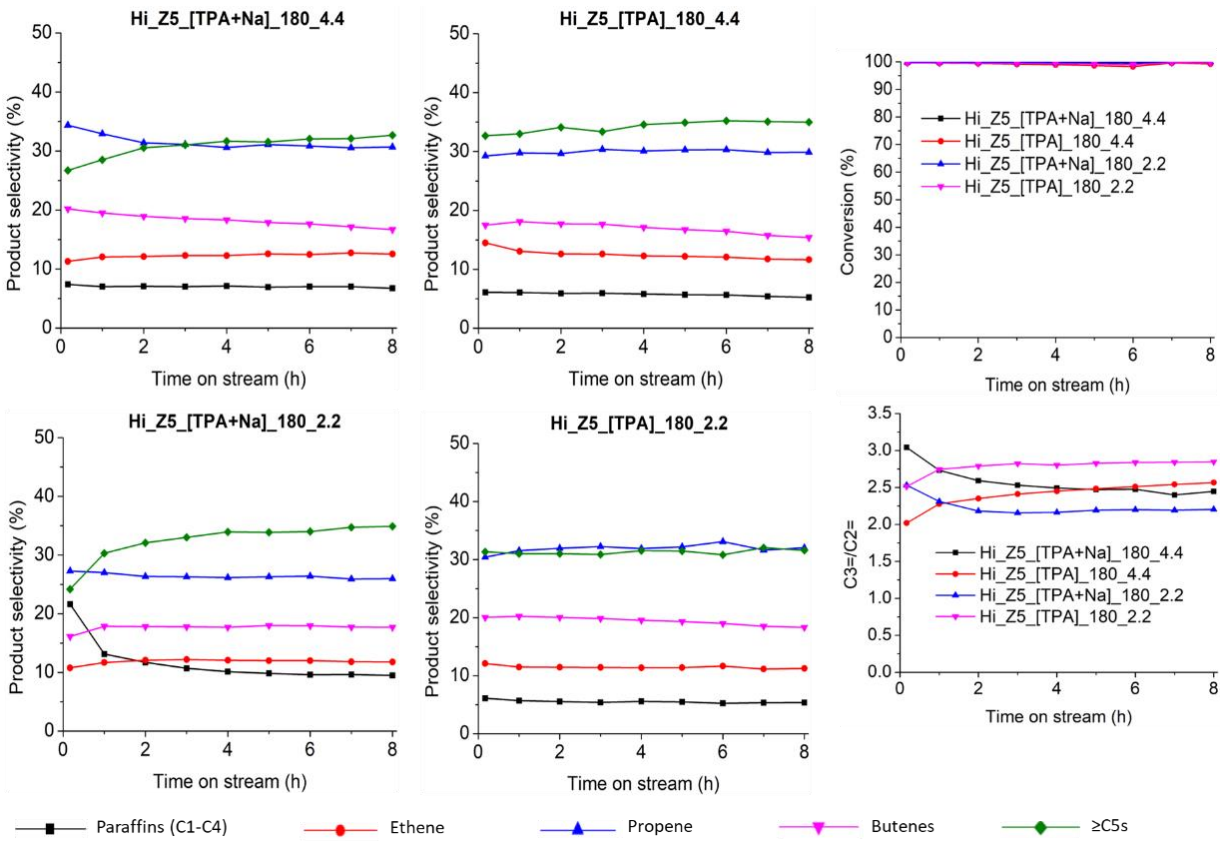

Figure 3.12. Product selectivity, ratio of C3=/C2= selectivities, and conversion of methanol with time on stream (TOS) over the hierarchical ZSM-5 with varied mesoporogen concentration.

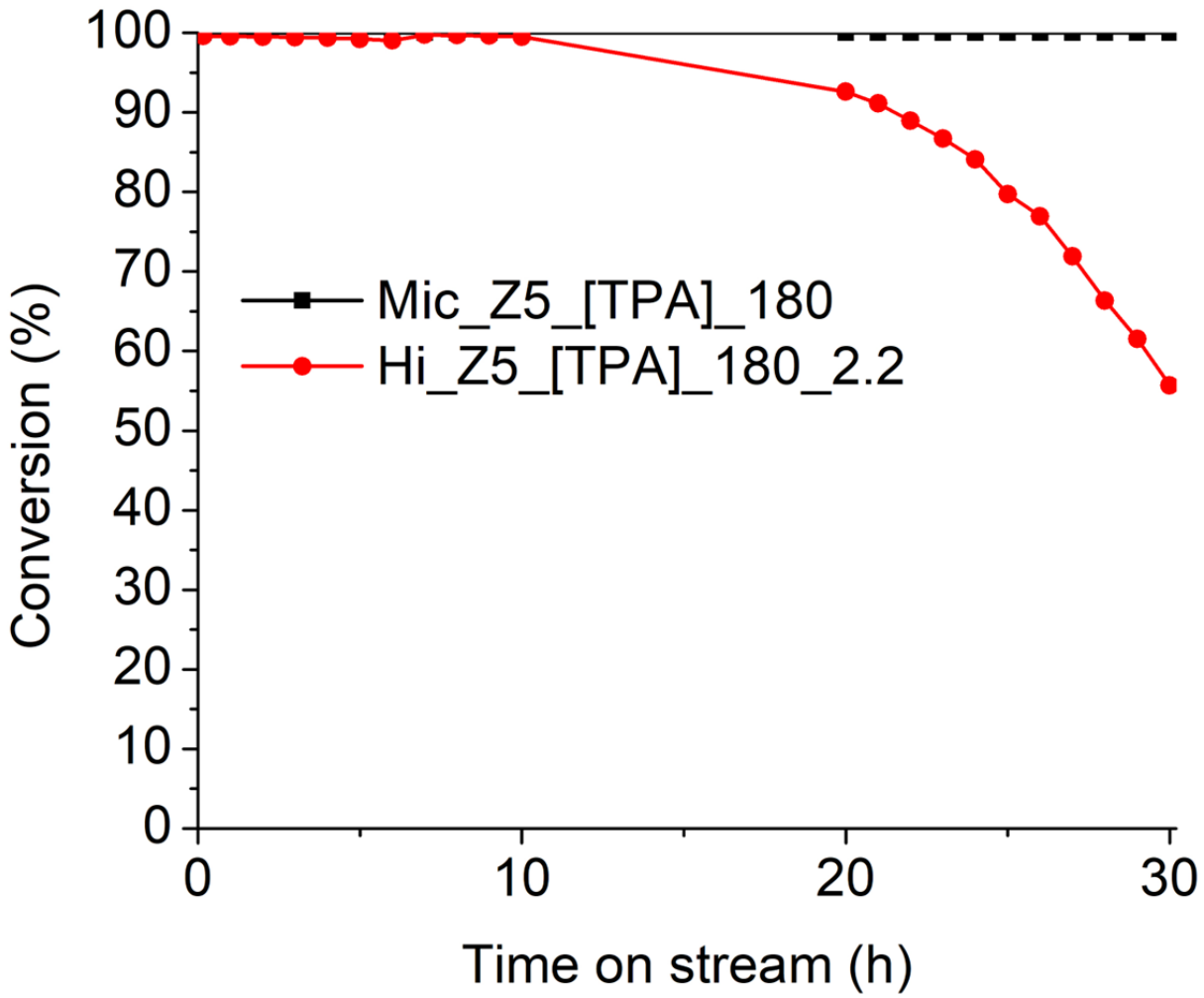

Figure 3.13. Methanol conversion with a long time on stream (TOS) over Mic_Z5_[TPA]_180 and Hi_Z5_[TPA]_180_2.2.

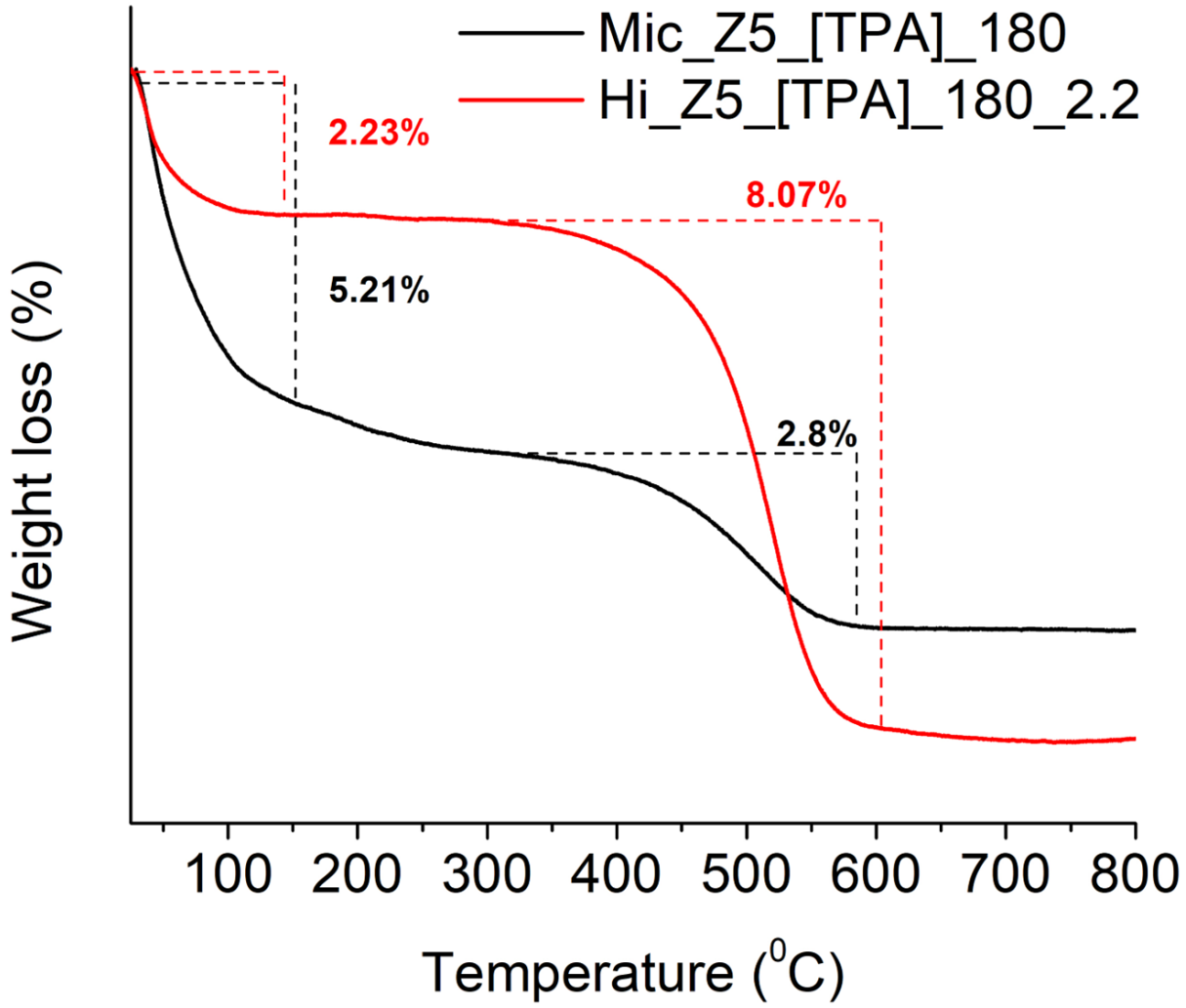

Figure 3.14. Thermogravimetry (TG) analysis of the used catalysts resulted from the methanol conversion reaction with TOS for 30 hours.

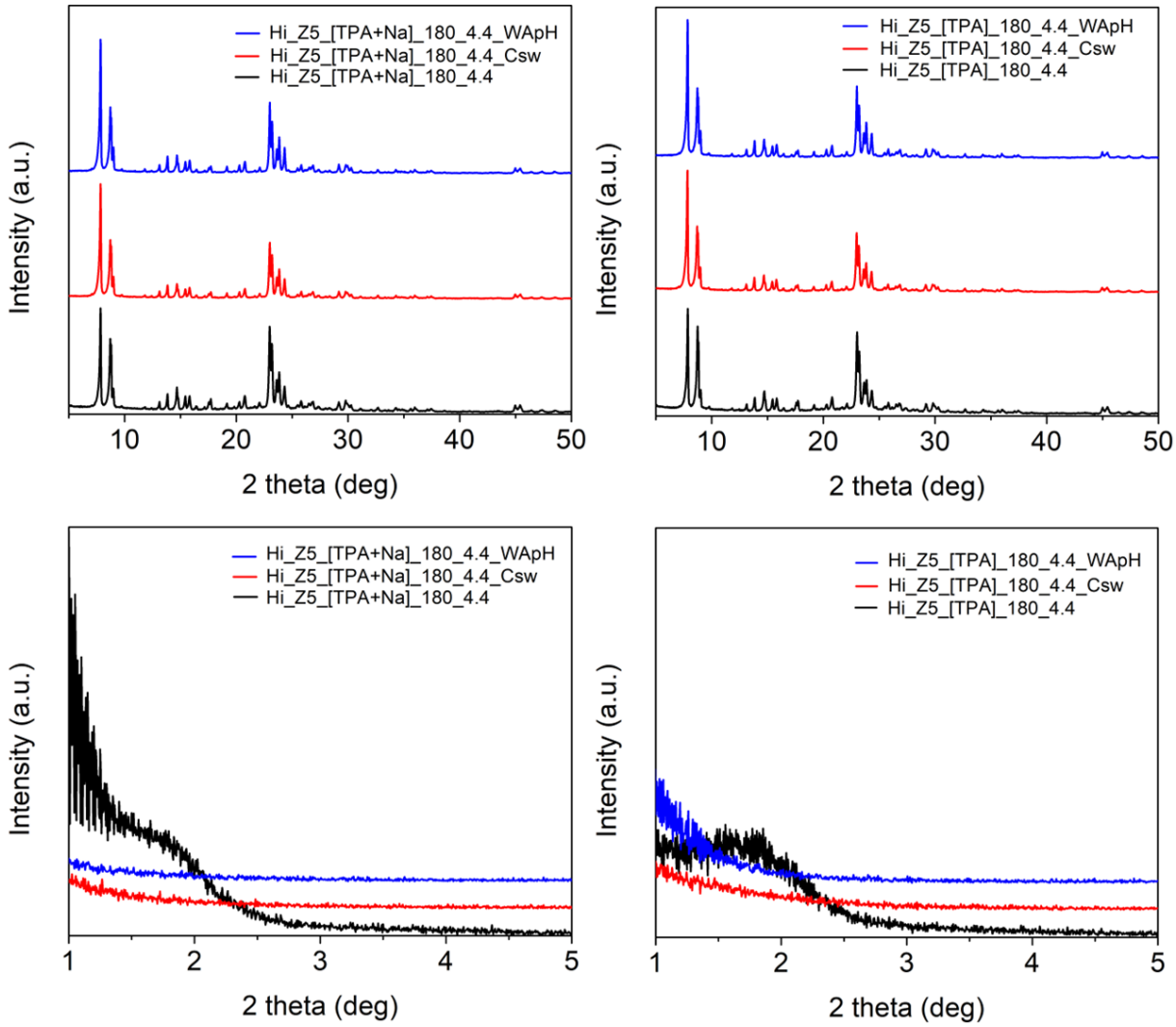

Figure 3.15. Wide and small angle patterns of XRD from the hierarchical ZSM-5 that the pH and timing mesoporogen addition varied.

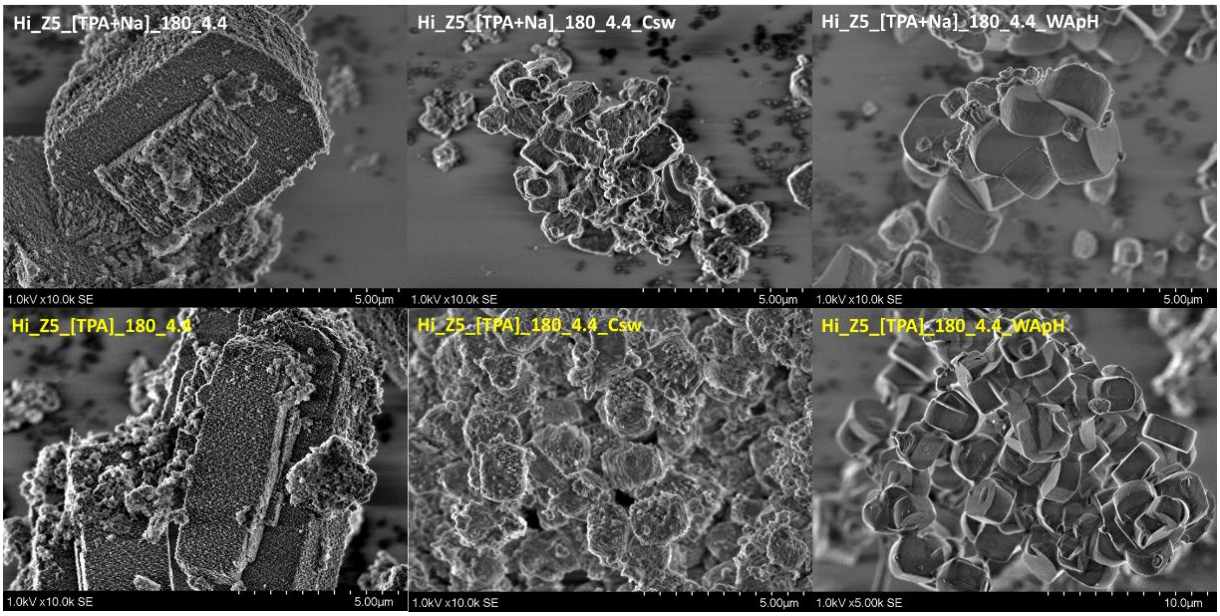

Figure 3.16. FE-SEM images from the hierarchical ZSM-5 that the pH and timing mesoporogen addition varied.

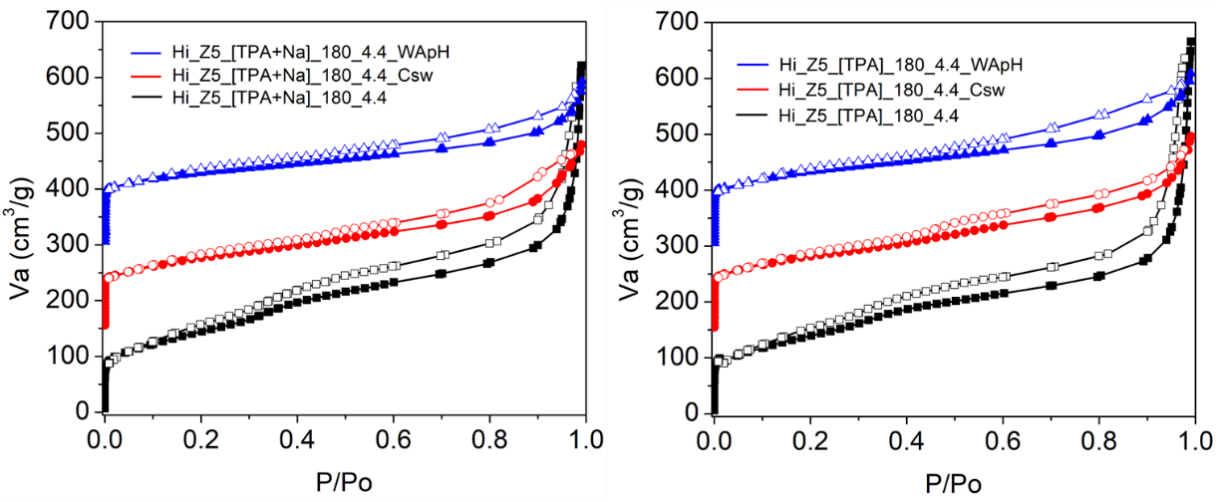

Figure 3.17. Isotherm of nitrogen adsorption and desorption from the hierarchical ZSM-5 that the pH and timing mesoporogen addition varied.

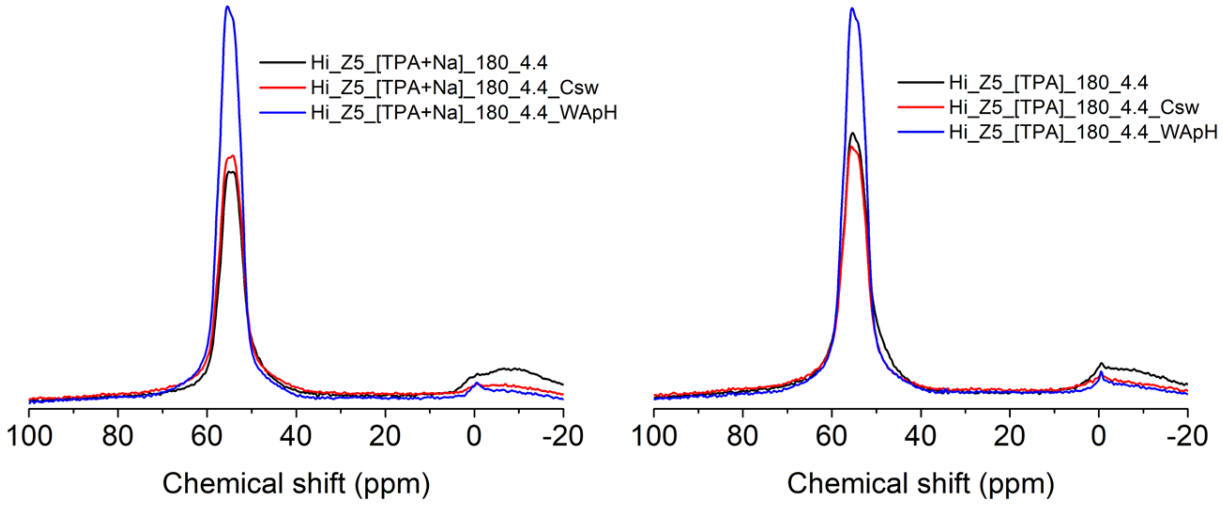

Figure 3.18. ^{27}Al MAS NMR spectra from the hierarchical ZSM-5 that the pH and timing mesoporogen addition varied.

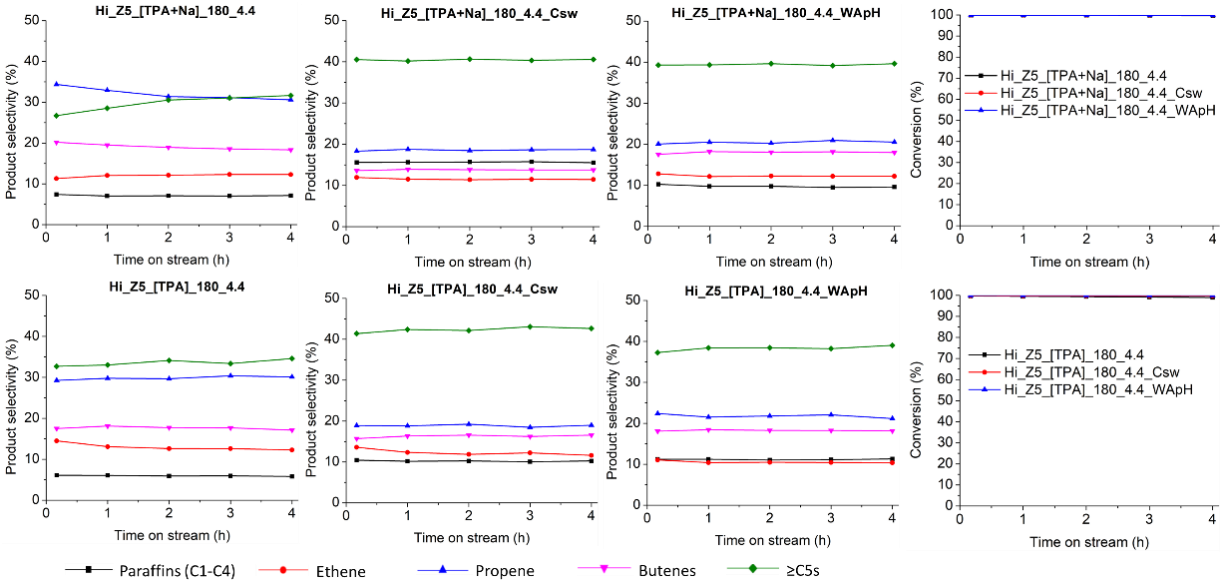

Figure 3.19. Methanol conversion and product selectivity with time on stream (TOS) over the hierarchical ZSM-5 that the pH and timing mesoporogen addition varied.

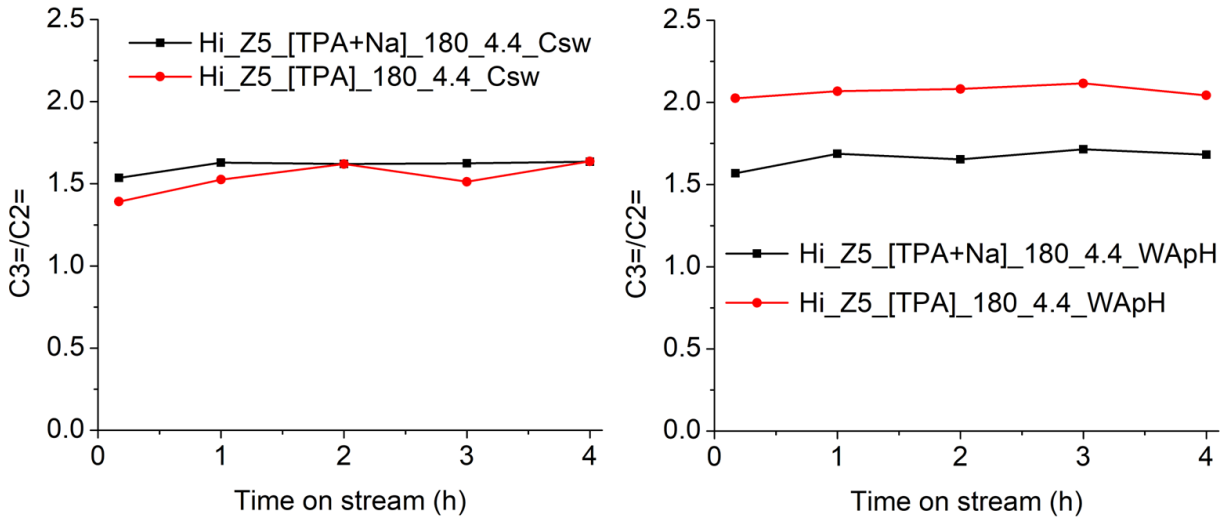

Figure 3.20. The ratio of C3=/C2= selectivity from the hierarchical ZSM-5 that the pH and timing mesoporogen addition varied.

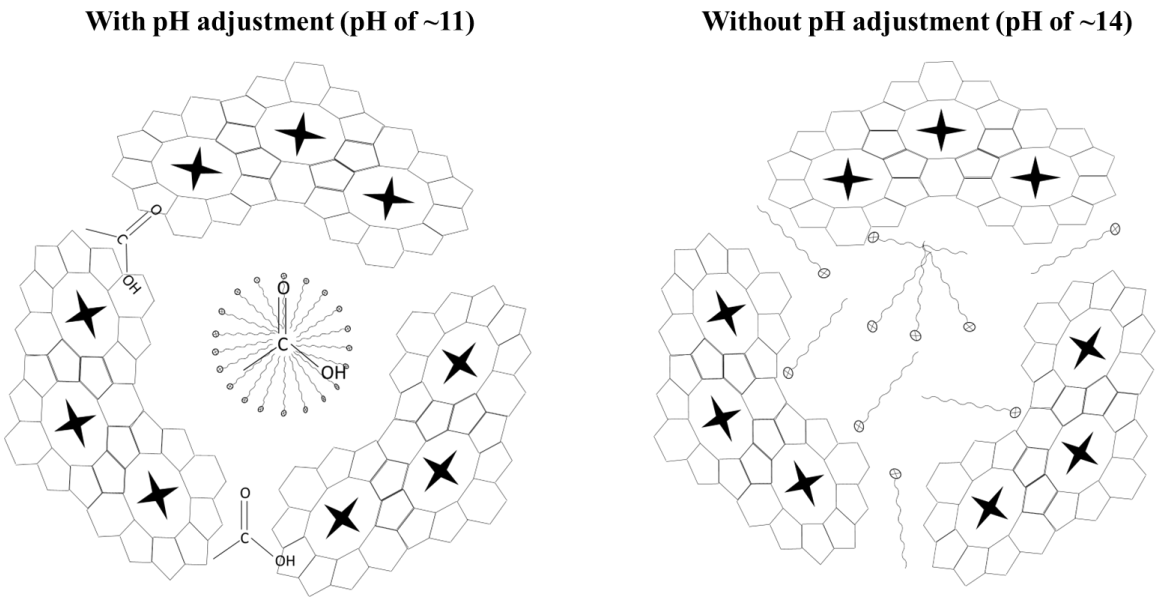

Figure 3.21. Possible interaction between the zeolite fragment, surfactant, and alcohol.

Table 3.1. The textural properties of the microporous and hierarchical ZSM-5s.

Sample	S_{BET} (m^2/g)[a]	S_{ext} (m^2/g)[b]	S_{meso} (m^2/g)[c]	S_{mic} (m^2/g)[d]	V_{mic} (cm^3/g)[b]	V_{meso} (cm^3/g)[e]	Pore size (nm)[f]	HF[g]
Mic_Z5_[TPA+Na]_180	425	35	121**	390*	0.17	0.26**	1.60	-
Mic_Z5_[TPA]_180	447	14	123**	433*	0.19	0.41**	1.49	-
Mic_Z5_[TPA+Na]_200	445	54	146**	391*	0.18	0.26**	1.80	-
Mic_Z5_[TPA]_200	471	71	191**	400*	0.21	0.28**	1.75	-
Hi_Z5_[TPA+Na]_180_4.4	519	140	208	171	0.06	0.22	2.71	0.06
Hi_Z5_[TPA]_180_4.4	504	156	194	154	0.05	0.18	2.54	0.05
Hi_Z5_[TPA+Na]_200_4.4	512	153	148	211	0.07	0.19	2.65	0.06
Hi_Z5_[TPA]_200_4.4	494	135	134	225	0.08	0.15	2.49	0.07

a: obtained by BET method.

b: calculated by t-plot method.

c: $S_{meso+ext} - S_{ext}$., where both derived from t-plot method.

d: $S_{BET} - S_{meso+ext}$.

e: $V_{meso+mic} - V_{mic}$, where both derived from t-plot method.

f: obtained by BJH method.

g: Hierarchy factor calculated from $(V_{mic}/V_{TPV})x(S_{BJH}/S_{BET})$; V_{TPV} = total pore volume calculated at P/P_0 0.99.

(*) $S_{mic} = S_{BET} - S_{ext}$, where *S*ext derived from t-plot.

(**) obtained from BJH method

Table 3.2. The chemical properties of all ZSM-5 zeolites.

Sample	Si/Al[a]	Strong Acid amount (µmol/g)[b]	FTIR-Pyr[c]			FTIR-Col[d]
			Brønsted (µmol/g)	Lewis (µmol/g)	B/L ratio	Brønsted (µmol/g)
Mic_Z5_[TPA+Na]_180	33	326	290	28	10.4	15.1
Mic_Z5_[TPA]_180	32	301	296	24	12.3	17.6
Mic_Z5_[TPA+Na]_200	34	303	288	21	13.7	14.6
Mic_Z5_[TPA]_200	32	190	171	71	2.41	28.2
Hi_Z5_[TPA+Na]_180_4.4	31	132	101	35	2.88	52.7
Hi_Z5_[TPA]_180_4.4	32	142	110	64	1.72	50.2
Hi_Z5_[TPA+Na]_200_4.4	33	124	102	44	2.32	53.6
Hi_Z5_[TPA]_200_4.4	34	118	109	39	2.79	53.6

a: obtained from ICP-AES.

b: obtained from NH_3-TPD

c: obtained at 250 ^{0}C

d= obtained at 100 ^{0}C

Table 3.3. The relative peak areas of the ^{27}Al MAS NMR spectra of the H-type samples from Gaussian function.

Sample	Al (a) 52 ppm	Al (b) 53 ppm	Al (c) 54 ppm	Al (d) 56 ppm	Al (e) 58 ppm	T_{56}/T_{54} Ratio
Mic_Z5_[TPA+Na]_180	9	20	25	30	16	1.20
Mic_Z5_[TPA]_180	11	22	26	30	10	1.15
Mic_Z5_[TPA+Na]_200	11	18	27	30	13	1.11
Mic_Z5_[TPA]_200	23	19	21	22	15	1.05
Hi_Z5_[TPA+Na]_180_4.4	12	20	24	24	20	1.00
Hi_Z5_[TPA]_180_4.4	13	14	15	22	35	1.47
Hi_Z5_[TPA+Na]_200_4.4	8	17	25	25	25	1.00
Hi_Z5_[TPA]_200_4.4	12	19	25	29	15	1.16

Table 3.4. Al pairs distribution of all samples determined from the Co-type samples were analyzed by Co(II) UV-Vis DRS.

Sample	Al pairs distribution (%)[b]		
	α	β	γ
Mic_Z5_[TPA+Na]_180	15	59	26
Mic_Z5_[TPA]_180	8	61	31
Mic_Z5_[TPA+Na]_200	12	55	33
Mic_Z5_[TPA]_200	6	68	26
Hi_Z5_[TPA+Na]_180_4.4	13	61	25
Hi_Z5_[TPA]_180_4.4	12	60	28
Hi_Z5_[TPA+Na]_200_4.4	2	75	23
Hi_Z5_[TPA]_200_4.4	4	72	24

Table 3.5. The textural properties from the hierarchical ZSM-5 with varied mesoporogen concentration.

Sample	S_{BET} (m^2/g)[a]	S_{ext} (m^2/g)[b]	S_{meso} (m^2/g)[c]	S_{mic} (m^2/g)[d]	V_{mic} (cm^3/g)[b]	V_{meso} (cm^3/g)[e]	Pore size (nm)[f]	HF[g]
Hi_Z5_[TPA+Na]_180_4.4	519	140	208	171	0.06	0.22	2.71	0.06
Hi_Z5_[TPA]_180_4.4	504	156	194	154	0.05	0.18	2.54	0.05
Hi_Z5_[TPA+Na]_180_2.2	469	106	163	200	0.08	0.14	2.49	0.08
Hi_Z5_[TPA]_180_2.2	496	144	118	234	0.08	0.14	2.33	0.08

a: obtained by BET method.

b: calculated by t-plot method.

c: $S_{meso+ext} - S_{ext}$., where both derived from t-plot method.

d: $S_{BET} - S_{meso+ext}$.

e: $V_{meso+mic} - V_{mic}$, where both derived from t-plot method.

f: obtained by BJH method.

g: Hierarchy factor calculated from $(V_{mic}/V_{TPV})x(S_{BJH}/S_{BET})$; V_{TPV} = total pore volume calculated at P/P_0 0.99.

Table 3.6. The chemical properties from the hierarchical ZSM-5 with varied mesoporogen concentration.

Sample	Si/Al[a]	Strong Acid amount (μmol/g)[b]	FTIR-Pyr[c]			FTIR-Col[d]
			Brønsted (μmol/g)	Lewis (μmol/g)	B/L ratio	Brønsted (μmol/g)
Hi_Z5_[TPA+Na]_180_4.4	31	132	101	35	2.88	52.7
Hi_Z5_[TPA]_180_4.4	32	142	110	64	1.72	50.2
Hi_Z5_[TPA+Na]_180_2.2	33	144	128	36	3.56	62.9
Hi_Z5_[TPA]_180_2.2	38	144	133	36	3.69	59.7

a: obtained from ICP-AES.

b: obtained from NH_3-TPD

c: obtained at 250 ^{0}C

d= obtained at 100 ^{0}C

Table 3.7. The relative peak areas of the ^{27}Al MAS NMR spectra from the H-type hierarchical ZSM-5 with varied mesoporogen concentration using the Gaussian function.

Sample	Al (a) 52 ppm	Al (b) 53 ppm	Al (c) 54 ppm	Al (d) 56 ppm	Al (e) 58 ppm	T_{56}/T_{54} Ratio
Hi_Z5_[TPA+Na]_180_4.4	12	20	24	24	20	1.00
Hi_Z5_[TPA]_180_4.4	13	14	15	22	35	1.47
Hi_Z5_[TPA+Na]_180_2.2	16	19	22	21	23	0.95
Hi_Z5_[TPA]_180_2.2	16	18	25	29	12	1.16

Table 3.8. Al pairs distribution of the hierarchical ZSM-5 with varied mesoporogen concentration determined from the Co-type samples was analyzed by Co(II) UV-Vis DRS.

Sample	Al pairs distribution (%)[b]		
	α	β	γ
Hi_Z5_[TPA+Na]_180_4.4	13	61	25
Hi_Z5_[TPA]_180_4.4	12	60	28
Hi_Z5_[TPA+Na]_180_2.2	10	71	19
Hi_Z5_[TPA]_180_2.2	10	68	22

Table 3.9. The pH of the mixture before the hydrothermal synthesis via the addition of acetic acetate.

Sample	Without pH adjustment	With pH adjustment
Hi_Z5_[TPA+Na]_180_4.4	~14	~11
Hi_Z5_[TPA]_180_4.4	~14	~11
Hi_Z5_[TPA+Na]_180_4.4_WApH	~14	~11
Hi_Z5_[TPA]_180_4.4_WApH	~14	~11

Table 3.10. The textural properties of the hierarchical ZSM-5 that the pH and timing mesoporogen addition varied.

Sample	S_{BET} (m^2/g)[a]	S_{ext} (m^2/g)[b]	S_{meso} (m^2/g)[c]	S_{mic} (m^2/g)[d]	V_{mic} (cm^3/g)[b]	V_{meso} (cm^3/g)[e]	Pore size (nm)[f]	HF[g]
Hi_Z5_[TPA+Na]_180_4.4	519	140	208	171	0.06	0.22	2.71	0.06
Hi_Z5_[TPA]_180_4.4	504	156	194	154	0.05	0.18	2.54	0.05
Hi_Z5_[TPA+Na]_180_4.4_Csw	454	149	54	251	0.09	0.08	1.75	0.12
Hi_Z5_[TPA]_180_4.4_Csw	471	149	38	284	0.10	0.09	1.75	0.13
Hi_Z5_[TPA+Na]_180_4.4_WApH	460	103	81	275	0.11	0.07	1.84	0.12
Hi_Z5_[TPA]_180_4.4_WApH	474	140	52	283	0.11	0.06	1.6	0.13

a: obtained by BET method.

b: calculated by t-plot method.

c: $S_{meso+ext} - S_{ext}$., where both derived from t-plot method.

d: $S_{BET} - S_{meso+ext}$.

e: $V_{meso+mic} - V_{mic}$, where both derived from t-plot method.

f: obtained by BJH method.

g: Hierarchy factor calculated from $(V_{mic}/V_{TPV})x(S_{BJH}/S_{BET})$; V_{TPV} = total pore volume calculated at P/P_0 0.99.

Table 3.11. The chemical properties from the hierarchical ZSM-5 that the pH and timing mesoporogen concentration varied.

Sample	Strong Acid amount (µmol/g)[a]	FTIR-Pyr[b]			FTIR-Col[c]
		Brønsted (µmol/g)	Lewis (µmol/g)	B/L ratio	Brønsted (µmol/g)
Hi_Z5_[TPA+Na]_180_4.4	132	101	35	2.88	52.7
Hi_Z5_[TPA]_180_4.4	142	110	64	1.72	50.2
Hi_Z5_[TPA+Na]_180_4.4_Csw	158	145	16	9.06	28.1
Hi_Z5_[TPA]_180_4.4_Csw	136	107	26	4.12	28.2
Hi_Z5_[TPA+Na]_180_4.4_WApH	204	231	29	7.97	9.3
Hi_Z5_[TPA]_200_4.4_WApH	173	219	30	7.3	16.0

a: obtained from NH_3-TPD

b: obtained at 250 ^{0}C

c: obtained at 100 ^{0}C

Table 3.12. The relative peak areas of the ^{27}Al MAS NMR spectra from the hierarchical ZSM-5 that the pH and timing mesoporogen concentration.

Sample	Al (a) 52 ppm	Al (b) 53 ppm	Al (c) 54 ppm	Al (d) 56 ppm	Al (e) 58 ppm	T_{56}/T_{54} Ratio
Hi_Z5_[TPA+Na]_180_4.4	12	20	24	24	20	1.00
Hi_Z5_[TPA]_180_4.4	13	14	15	22	35	1.47
Hi_Z5_[TPA+Na]_180_4.4_Csw	12	19	23	25	21	1.09
Hi_Z5_[TPA]_180_4.4_Csw	10	15	17	18	40	1.06
Hi_Z5_[TPA+Na]_180_4.4_WApH	8	15	24	27	26	1.13
Hi_Z5_[TPA]_180_4.4_WApH	7	16	24	29	24	1.21

Table 3.13. Al pairs distribution of the hierarchical ZSM-5 that the pH and timing mesoporogen addition varied from the Co-type samples was analyzed by Co(II) UV-Vis DRS.

Sample	Al pairs distribution (%)[b]		
	α	β	γ
Hi_Z5_[TPA+Na]_180_4.4	13	61	25
Hi_Z5_[TPA]_180_4.4	12	60	28
Hi_Z5_[TPA+Na]_180_4.4_Csw	13	65	22
Hi_Z5_[TPA]_180_4.4_Csw	4	70	26
Hi_Z5_[TPA+Na]_180_4.4_WApH	6	69	26
Hi_Z5_[TPA]_180_4.4_WApH	5	71	21

3.6. References

[1] S. Wang, P. Wang, Z. Qin, Y. Chen, M. Dong, J. Li, K. Zhang, P. Liu, J. Wang, W. Fan, Relation of catalytic performance to the aluminum siting of acidic zeolites in the conversion of methanol to olefins, viewed via a comparison between ZSM-5 and ZSM-11, ACS Catal. 8 (2018) 5485–5505.

[2] J. Chen, T. Liang, J. Li, S. Wang, Z. Qin, P. Wang, L. Huang, W. Fan, J. Wang, Regulation of Framework Aluminum Siting and Acid Distribution in H-MCM-22 by Boron Incorporation and Its Effect on the Catalytic Performance in Methanol to Hydrocarbons, ACS Catal. 6 (2016) 2299–2313.

[3] Q. Zhu, J.N. Kondo, T. Yokoi, T. Setoyama, M. Yamaguchi, T. Takewaki, K. Domen, T. Tatsumi, The influence of acidities of boron- and aluminium-containing MFI zeolites on co-reaction of methanol and ethene, Phys. Chem. Chem. Phys. 13 (2011) 14598–14605.

[4] M. Liu, T. Yokoi, M. Yoshioka, H. Imai, J.N. Kondo, T. Tatsumi, Differences in Al distribution and acidic properties between RTH-type zeolites synthesized with OSDAs and without OSDAs, Phys. Chem. Chem. Phys. 16 (2014) 4155–4164.

[5] J.R. Di Iorio, R. Gounder, Controlling the Isolation and Pairing of Aluminum in Chabazite Zeolites Using Mixtures of Organic and Inorganic Structure-Directing Agents, Chem. Mater. 28 (2016) 2236–2247.

[6] Y. Wang, T. Yokoi, S. Namba, J.N. Kondo, T. Tatsumi, Improvement of catalytic performance of MCM-22 in the cracking of n-hexane by controlling the acidic property, J. Catal. 333 (2016) 17–28.

[7] S.M. Maier, A. Jentys, J.A. Lercher, Steaming of zeolite BEA and its effect on acidity:

A comparative NMR and IR spectroscopic study, J. Phys. Chem. C. 115 (2011) 8005–8013.

[8] S. Kim, G. Park, M.H. Woo, G. Kwak, S.K. Kim, Control of Hierarchical Structure and Framework-Al Distribution of ZSM-5 via Adjusting Crystallization Temperature and Their Effects on Methanol Conversion, ACS Catal. 9 (2019) 2880–2892.

[9] J. Rouquerol, P. Llewellyn, F. Rouquerol, Is the BET equation applicable to microporous adsorbents?, Elsevier B.V., 2007.

[10] S. Bosnar, V. Rac, D. Stošić, A. Travert, G. Postole, A. Auroux, S. Škapin, L. Damjanović-Vasilić, J. Bronić, X. Du, S. Marković, V. Pavlović, V. Rakić, Overcoming phase separation in dual templating: A homogeneous hierarchical ZSM-5 zeolite with flower-like morphology, synthesis and in-depth acidity study, Microporous Mesoporous Mater. 329 (2022).

[11] H. Yamazaki, H. Shima, H. Imai, T. Yokoi, T. Tatsumi, J.N. Kondo, Evidence for a "carbene-like" intermediate during the reaction of methoxy species with light alkenes on H-ZSM-5, Angew. Chemie - Int. Ed. 50 (2011) 1853–1856.

[12] H. Yamazaki, H. Shima, H. Imai, T. Yokoi, T. Tatsumi, J.N. Kondo, Direct production of propene from methoxy species and dimethyl ether over H-ZSM-5, J. Phys. Chem. C. 116 (2012) 24091–24097.

[13] M. Guisnet, P. Ayrault, C. Coutanceau, M.F. Alvarez, J. Datka, Acid properties of dealuminated beta zeolites studied by IR spectroscopy, J. Chem. Soc. - Faraday Trans. 93 (1997) 1661–1665.

[14] J. Ding, J. Hu, T. Xue, Y. Wang, H. Wu, P. Wu, M. He, Direct synthesis of self-assembled ZSM-5 microsphere with controllable mesoporosity and its enhanced LDPE

cracking properties, RSC Adv. 6 (2016) 38671–38679.

[15] S. Namba, S. Nakanishi, T. Yashima, Behavior of quinoline derivatives as poisons in isomerization of p-xylene on HZSM-5 zeolite, J. Catal. 88 (1984) 505–508.

[16] Y.K. Krisnandi, B.A.P. Putra, M. Bahtiar, Zahara, I. Abdullah, R.F. Howe, Partial Oxidation of Methane to Methanol over Heterogeneous Catalyst Co/ZSM-5, Procedia Chem. 14 (2015) 508–515.

[17] L. Yu, J. Zhou, W. Wang, Sub-micron sized hierarchical porous ZSM-5 particles with controllable mesoporous structures by changing the alkalinity in the synthesis using NaOH, J. Solid State Chem. 322 (2023) 123989.

[18] J.S. Beck, J.C. Vartuli, W.J. Roth, M.E. Leonowicz, C.T. Kresge, K.D. Schmitt, C.T.W. Chu, D.H. Olson, E.W. Sheppard, S.B. McCullen, J.B. Higgins, J.L. Schlenker, A New Family of Mesoporous Molecular Sieves Prepared with Liquid Crystal Templates, J. Am. Chem. Soc. 114 (1992) 10834–10843.

[19] G. Leofanti, M. Padovan, G. Tozzola, B. Venturelli, Surface area and pore texture of catalysts, Catal. Today. 41 (1998) 207–219.

[20] S. Wang, T. Dou, Y. Li, Y. Zhang, X. Li, Z. Yan, A novel method for the preparation of MOR/MCM-41 composite molecular sieve, Catal. Commun. 6 (2005) 87–91.

[21] D.P. Serrano, R.A. García, G. Vicente, M. Linares, D. Procházková, J. Čejka, Acidic and catalytic properties of hierarchical zeolites and hybrid ordered mesoporous materials assembled from MFI protozeolitic units, J. Catal. 279 (2011) 366–380.

[22] J. Na, G. Liu, T. Zhou, G. Ding, S. Hu, L. Wang, Synthesis and catalytic performance of ZSM-5/MCM-41 zeolites with varying mesopore size by surfactant-directed recrystallization, Catal. Letters. 143 (2013) 267–275.

[23] J. Peréz-Ramírez, D. Verboekend, A. Bonilla, S. Abelló, Zeolite catalysts with tunable hierarchy factor by pore-growth moderators, Adv. Funct. Mater. 19 (2009) 3972–3979.

[24] M.K. Wardani, G.T.M. Kadja, A.T.N. Fajar, Subagjo, I.G.B.N. Makertihartha, M.L. Gunawan, V. Suendo, R.R. Mukti, Highly crystalline mesoporous SSZ-13 zeolite obtained via controlled post-synthetic treatment, RSC Adv. 9 (2019) 77–86.

[25] F. Thibault-Starzyk, A. Vimont, J.P. Gilson, 2D correlation IR spectroscopy of xylene isomerisation on H-MFI zeolite, Stud. Surf. Sci. Catal. 135 (2001) 133.

[26] T. Biligetu, Y. Wang, T. Nishitoba, R. Otomo, S. Park, H. Mochizuki, J.N. Kondo, T. Tatsumi, T. Yokoi, Al distribution and catalytic performance of ZSM-5 zeolites synthesized with various alcohols, J. Catal. 353 (2017) 1–10.

[27] T. Yokoi, H. Mochizuki, S. Namba, J.N. Kondo, T. Tatsumi, Control of the Al Distribution in the Framework of ZSM-5 Zeolite and Its Evaluation by Solid-State NMR Technique and Catalytic Properties, J. Phys. Chem. C. 119 (2015) 15303–15315.

[28] J. Dědeček, Z. Sobalík, B. Wichterlová, Siting and Distribution of Framework Aluminium Atoms in Silicon-Rich Zeolites and Impact on Catalysis, Catal. Rev. - Sci. Eng. 54 (2012) 135–223.

[29] T. Liang, J. Chen, Z. Qin, J. Li, P. Wang, S. Wang, G. Wang, M. Dong, W. Fan, J. Wang, Conversion of Methanol to Olefins over H-ZSM-5 Zeolite: Reaction Pathway Is Related to the Framework Aluminum Siting, ACS Catal. 6 (2016) 7311–7325.

[30] S. Svelle, P.O. Rønning, S. Kolboe, Kinetic studies of zeolite-catalyzed methylation reactions: 1. Coreaction of [12C]ethene and [13C]methanol, J. Catal. 224 (2004) 115–123.

[31] S. Ilias, A. Bhan, Mechanism of the catalytic conversion of methanol to hydrocarbons,

ACS Catal. 3 (2013) 18–31.

[32] S. Ilias, A. Bhan, The mechanism of aromatic dealkylation in methanol-to-hydrocarbons conversion on H-ZSM-5: What are the aromatic precursors to light olefins?, J. Catal. 311 (2014) 6–16.

[33] X. Mi, Z. Hou, X. Li, H. Liu, X. Guo, Synergistic effect between organic structure-directing agent and crystal seed toward controlled morphology, and bimodal pore structure of aggregated nanosized ZSM-5, Microporous Mesoporous Mater. 302 (2020) 110255.

[34] J. Wang, C. Liu, P. Zhu, H. Liu, X. Zhang, Y. Zhang, J. Liu, L. Zhang, W. Zhang, Synthesis of hierarchical ZSM-5 nano-aggregated microspheres for application in enhancing the stability of n -hexane aromatization, New J. Chem. 45 (2021) 18659–18668.

[35] R.M. Barrer, Zeolites and their synthesis, Zeolites. 1 (1981) 130–140.

[36] Q. Huo, R. Leon, P.M. Petroff, G.D. Stucky, Mesostructure design with gemini surfactants: Supercage formation in a three-dimensional hexagonal array, Science (80-.). 268 (1995) 1324–1327.

[37] F.N. Gu, F. Wei, J.Y. Yang, N. Lin, W.G. Lin, Y. Wang, J.H. Zhu, New strategy to synthesis of hierarchical mesoporous zeolites, Chem. Mater. 22 (2010) 2442–2450.

Chapter 4

Summary and acknowledgments

Summary

Chapter 2:

Adjustment of aluminum distribution had been carried out on the hierarchical ZSM-5 intracrystalline. It was found that aluminum more located in the channel intersections than in the channels was produced by the hierarchical ZSM-5 with Na, which is opposite to the microporous ZSM-5's trend. The hierarchical ZSM-5 using a surfactant as mesoporogen gave rise to the occurrence of Al migration process from the micropores to mesopores and/or the external surface. Meanwhile, prolonging the hydrothermal time until 144 h resulted in not only a more well-structured hierarchical structure but also better chemical properties, which increased the hierarchy factor and strength of acid sites in the zeolite. Furthermore, it also influenced the rate of Al migration. The impact of the framework structure and the controlled aluminum was also seen in MTO and *n*-hexane cracking reactions. The hierarchical structure was predominant in producing lower olefins, especially in propene, compared to the micropore only, in which the hierarchical ZSM-5 without Na was superior to that with Na. This work provides valuable insights into the development of various hierarchical zeolite catalysts using a surfactant as mesoporogen with the location of aluminum controlled in the pores to enhance the catalytic performances.

Chapter 3:

The effect of the synthesis condition and the composition of the starting materials on the aluminum distribution in the hierarchical ZSM-5 intracrystalline has been investigated. For the parameter of the crystallization temperature, the high crystallization temperature influenced not only aluminum distribution in the framework but also the hierarchical structure. Overheating crystallization temperature resulted in the enhancement of Al pairs distribution in the channel intersections, with a higher concentration on Hi_Z5_[TPA+Na]. However, the high

crystallization temperature did not influence the ratio of Al distribution on the channels to the channel intersections, but it impacted on Hi_Z5_[TPA]. Moreover, a high crystallization temperature gave rise to an inhomogeneous structure between the microporous structure and mesoporous structure. In addition, it would lead to the formation of the microporous structure. Whereas for the parameter of the synthetic gel pH, the hierarchical ZSM-5 without pH adjustment (pH of ~14) possessed Al distribution was more concentrated in the channel intersection for Hi_Z5_[TPA+Na]_180_4.4_WApH, like the hierarchical ZSM-5 with pH adjustment which supported by ratio of T_{56}/T_{54} in the framework and ratio of C3=/C2= selectivity in the reaction of methanol conversion. Furthermore, the high pH of synthetic gel resulted in an increase of Al pairs distribution in the channel intersections. Meanwhile, the hierarchical structure produced by this treatment was not achieved. Even, it tends to the formation of the microporous structure only. On the other hand, Al distribution produced by the hierarchical ZSM-5 with timing mesoporogen addition into the synthetic gel switched to microporogen demonstrated the reversed trend with the hierarchical ZSM-5 synthesized using the original procedure. Its trend was the same as the original ZSM-5, in which the sample containing sodium (Hi_Z5_[TPA+Na]_180_4.4_Csw) had a higher ratio of T_{56}/T_{54} than the sample without containing sodium (Hi_Z5_[TPA+Na]_180_4.4_Csw). This result was also supported by the ratio of C3=/C2= selectivity in the methanol conversion, in which Hi_Z5_[TPA+Na]_180_4.4_Csw exhibited a higher ratio. Moreover, it resulted in a higher percentage of Al pairs distribution in the channel intersections compared to the control samples. Whereas the produced hierarchical structure, this treatment produced the mesopore inside the framework very little, which was shown by the appearance of a very low mesoporous step, indicating the microporous structure was more dominant than the mesoporous structure.

For the parameter of the composition of the starting materials, Al distribution on the hierarchical ZSM-5 with a lower concentration of mesoporogen (Hi_Z5_[TPA+Na]_180_2.2

and Hi_Z5_[TPA]_180_2.2) demonstrated the same trend as the hierarchical ZSM-5 with a higher concentration, in which Al distribution on Hi_Z5_[TPA+Na]_180_2.2 was more located in the channel intersections than Hi_Z5_[TPA]_180_2.2. This result was supported by the ratio of C3=/C2= selectivity in the methanol conversion reaction was higher on Hi_Z5_[TPA]_180_2.2. Furthermore, the produced Al pairs distribution in the channel intersections was higher than the hierarchical ZSM-5 with a higher concentration, indicating the low concentration of mesoporogen would force the formation of Al pairs. In short, this study gives valuable insight into the development of various zeolite catalysts (particularly in the hierarchical ZSM-5 zeolite) in terms of the correlation between the synthesis condition and the composition of the starting material toward aluminum distribution in the ZSM-5 zeolite to increase the selectivity of the catalytic process.

Based on findings in Chapter 2 and 3, it can be concluded that modification of ZSM-5 zeolite has been successfully conducted, either modification on the framework structure or modification on the aluminum distribution in the framework. The hierarchical ZSM-5 intracrystalline could be achieved by adjusting the pH of the synthetic gel (pH of ~11). Meanwhile, the homogeneity between the microporous structure and mesoporous structure could be carried out by prolonging the crystallization time for 144 h at a moderate crystallization temperature (160 ^{0}C) with the mesoporogen concentration of 4.4 mol. Whereas at high crystallization temperature and low concentration of mesoporogen, the degree of homogeneity decreased, by the process of the structure formation led to the micropore. Meanwhile, modification of aluminum distribution on the hierarchical ZSM-5 intracrystalline could be achieved in simple ways, i.e., addition or without the addition of sodium in the synthetic gel. By adding sodium into the synthetic gel, the aluminum distribution would be more concentrated in the channel intersections, and the Al pairs distribution in that location was increased. Even, by changing the crystallization temperature to a higher degree, the

mesoporogen concentration to a lower value, the pH of the synthetic gel to a higher value, timing the mesoporogen addition into the synthetic gel, the percentage of Al pairs distribution in the channel intersections would be significantly enhanced. Furthermore, the impact of those modifications resulted in an enhancement in product selectivity on the reaction of *n*-hexane cracking and methanol conversion, in which the hierarchical ZSM-5 (particularly on the hierarchical ZSM-5 without Na) demonstrated more selective to produce propene than the original ZSM-5.

In conclusion, this work gives valuable insights into the zeolite field, especially the field of hierarchical zeolite, as a catalyst for increasing product selectivity in catalytic processes.

List of publications

1. **Tahta M. Karim**, Hiroto Toyoda, Masato Sawada, Liang Zhao, Yong Wang, Peipei Xiao, Lizhuo Wang, Jun Huang, and Toshiyuki Yokoi. Aluminum Distribution on the Microporous and Hierarchical ZSM-5 Intracrystalline and its Impact on the Catalytic Performance. Chem & Bio Engineering, accepted (be-2024-00117n.R2) (Chapter 2).
2. Liang Zhao, Pei-pei Xiao, Yong Wang, Yao Lu, **Tahta Muslim Karim**, Herman Gies, and Toshiyuki Yokoi. “Modulation of Al distribution in High-Silica ZSM-5 Zeolites for Enhancing Catalytic Performance”. ACS Appl. Mater. Interfaces 2024, 16, 17701-17714.

List of conference presentations

1. T. M. Karim, Y. K. Krisnandi, Y. Wang, T. Yokoi. International Symposium on Porous Material, 2022. (Poster).
2. Tahta Muslim Karim, Nandkisor Urkude, Toshiyuki Yokoi. 5th Euro Asia Zeolite Conferene, 2022. (Poster).
3. T. M. Karim, U. Nandkisor, L. Zhao, T. Yokoi. International Symposium on Porous Material, 2023. (Poster).

Acknowledgment

As long as I registered as a student at the Tokyo Institute of Technology, I faced many challenges and happiness. The COVID-19 era is the biggest challenge in my study career due to I must stay in my country for 2 years without being able to do the experiment at all. While, my biggest happiness is when I (finally) meet many people from various countries in the laboratory possessing the same interest, i.e., zeolite. They are very kind and helpful in tackling technical problems in the lab and boosting my knowledge via scientific discussion. Without their help, this thesis would never have come to be.

First, I would like to thank God (Allah SWT), who blessed me with peace of mind and a wealth of knowledge. Moreover, I would like to express my sincere gratitude to my supervisor Prof. Toshiyuki Yokoi, who give me invaluable guidance and a spirit encouragement throughout this study, and the financial support. Then, I would like to thank my parents, who always give me strength, either moral or spiritual. Also, I would like to express my thanks to all my friends in the lab, particularly Nandkisor and Zhao, who are always ready to help me anytime and anywhere.

Finally, Pondok Pesantren Al Fattah, Siman, Lamongan, Indonesia, is highly acknowledged for giving me financial support for my studies. I must also thank my girlfriend, who always gives me steadfast support and the spirit and moral encouragement. Without her, I would feel lonely and stressed during my time in Japan.